



UNIVERSIDAD MICHOCANA
DE SAN NICOLÁS DE HIDALGO

Advanced Techniques of X-ray Fluorescence Spectrometry and their Applications

Nabanita Dasgupta-Schubert

Department of Physics and Mathematics
University of Michoacan, Morelia, Mexico

International School NUMAR-2024

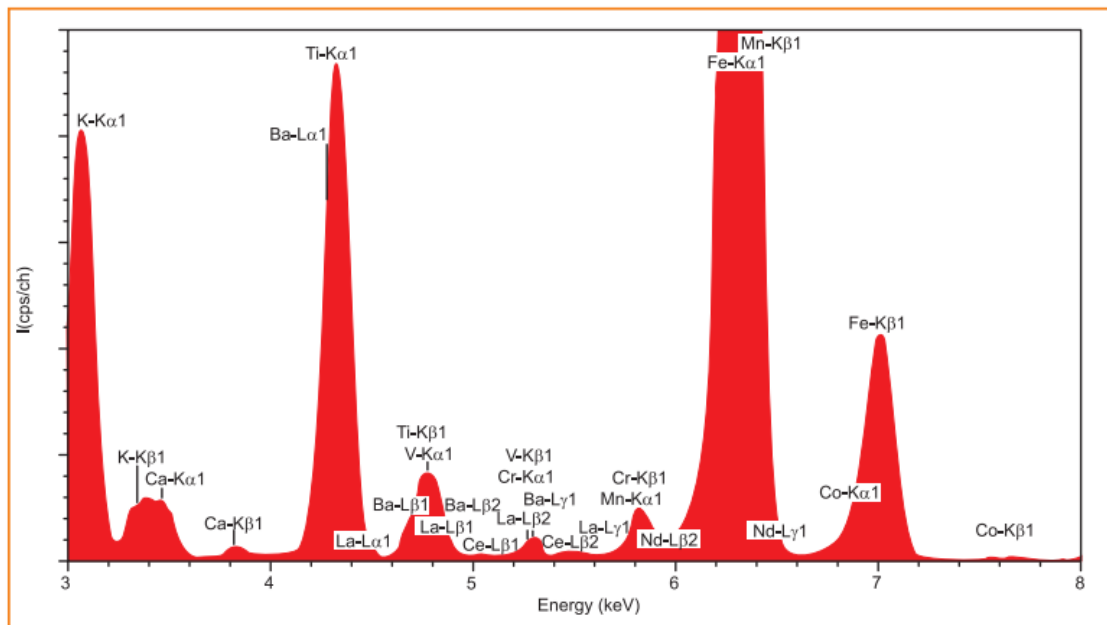


I.1 Xray Fluorescence (XRF) Spectrometry

- XRF spectrometry: qualitative and quantitative elemental analysis technique with broad application in science and industry.
- One of the most common non-destructive elemental analysis techniques.
- Based on the interaction between X-ray photons and matter:
 - emission of characteristic radiation (fluorescence) that is unique for every element. By counting the number of photons of each energy emitted from a sample, the elements present can be identified and quantitated.
- 2 common techniques: Energy Dispersive EDXRF and Wavelength Dispersive (WDXRF).
 - EDXRF: the energies of fluoresced x-rays is collected and recorded by a detector and the spectrum displayed in the energy discriminated mode.
Analyte range, Na-U
 - WDXRF: a crystal or other diffracting device separates the fluoresced x-rays by wavelength which are then collected and recorded by a detector. Analyte range, Be-U.
 - This lecture will focus on EDXRF spectrometry
- Concentration range sub-ppm (advanced XRF techniques) to 100%
- Detection limit depends upon the specific element and the sample matrix but in general for heavy elements the limit of detection (LLD) is superior.

- High precision and reproducibility. High accuracies, especially when good standard specimens are available.
- Measurement time depends on the number of elements to be determined and the degree of accuracy. Between a few seconds to 30 mins. Instrument analysis time after measurement is a few seconds.

Fig. 1 shows the EDXRF of a typical soil sample. The position of the peaks w.r.t energy identifies the element. The peak areas quantify the amount of the element present.



I.2 Production of X-rays in XRF spectrometry

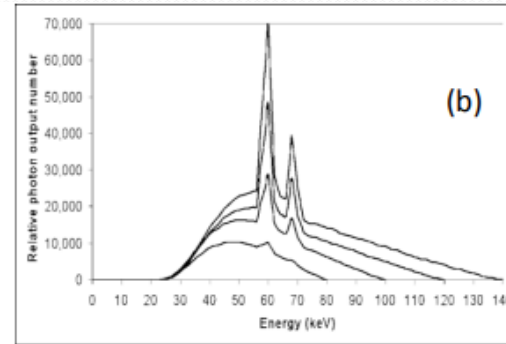
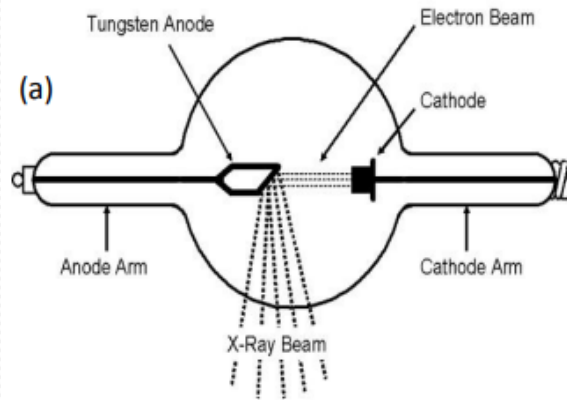
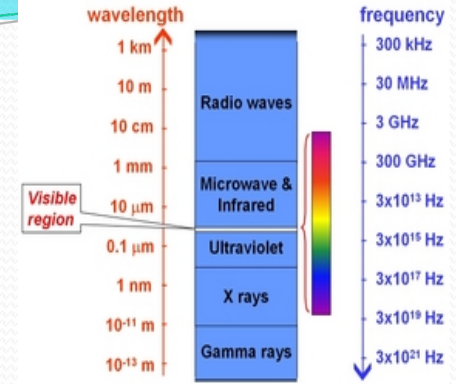
X-rays are a form of high energy EM radiation.

λ 150Å to $\sim < 0.02\text{Å} \equiv E \sim 100 \text{ eV}$ to 100s of keV

For a given photon, $E = h\nu = hc/\lambda$ where h is Planck's constant and c is the velocity of light.

X-rays can be produced by a radioactive source (e.g. ^{55}Fe), an x-ray tube or a synchrotron (a particular type of cyclic particle accelerator). Most laboratory XRF studies are done with x-ray tubes.

A schematic diagram of typical x-ray tube with a W anode (fig. 2a) and its x-ray emission spectrum at different HV (fig. 2b)



Broad continuum - Bremsstrahlung radiation (BR). Result of decelerating electron in the Coulomb field of the anode's atoms.

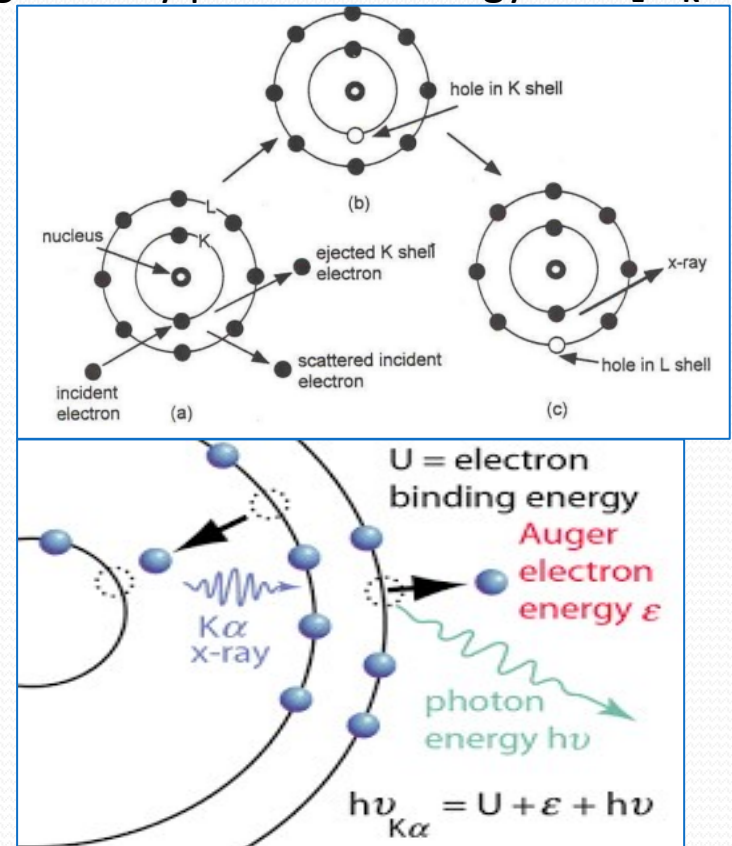
$E_{\text{max}} = eU$ where E_{max} = max energy of the BR, e = electronic charge, $U = HV$.

e.g. if U is 40 kV, $E_{\text{max}} = 40 \text{ keV}$

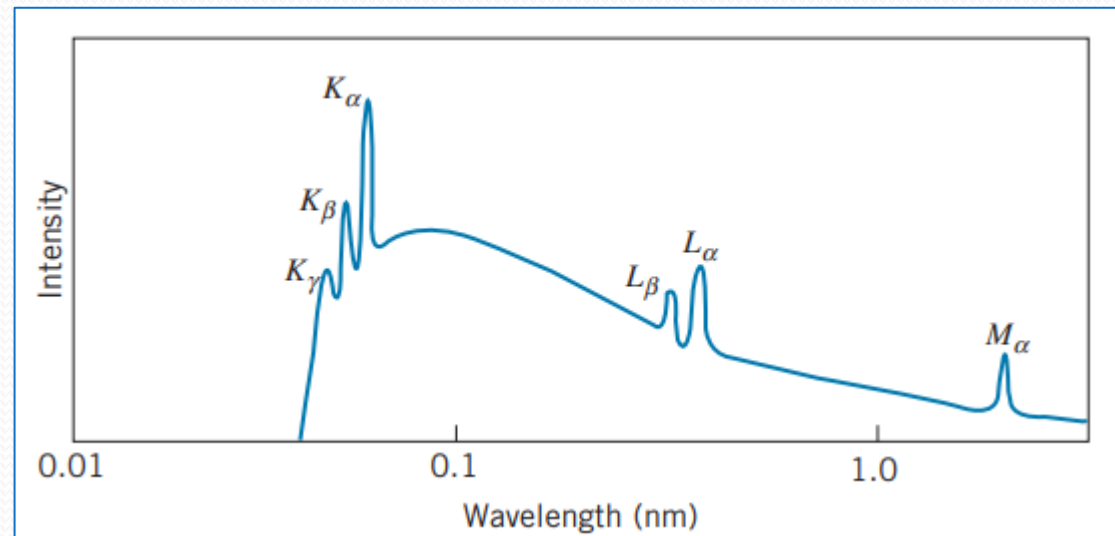
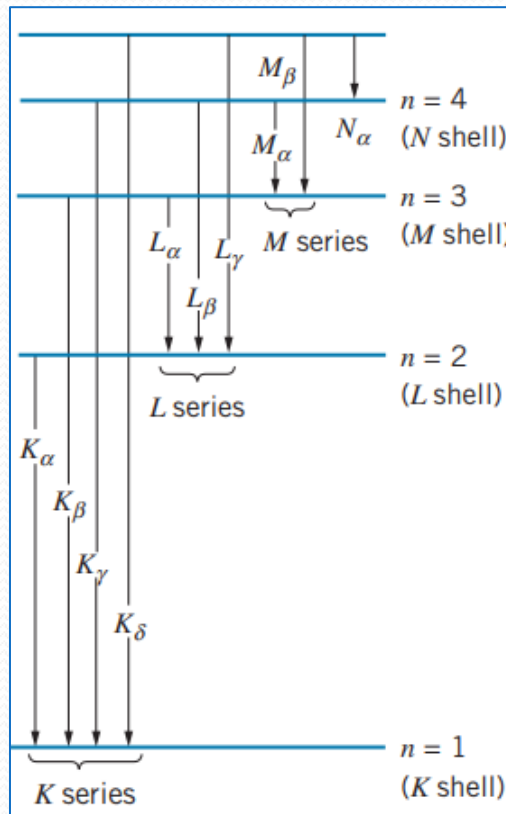
Sharp peaks on top of BR = Characteristic radiation (CR) of the element of the anode (Tungsten)

I.3 Xray Transitions and Moseley's Law

- The xray photon is emitted in electronic transitions between the more tightly bound inner electron energy levels of an atom.
- The energy of the photon is the difference in energy of the 2 atomic levels involved.
 - Example: An e- from the n=1 shell (K shell) is ejected by energetic particle collision (e.g. electron scattering or photoelectric process), then an upper bound state e-, e.g from the n=2 or L shell, fills that vacancy, emitting an x-ray photon of energy $E = E_L - E_K$
- Auger e- production (fig. 3b): The fluoresced x-ray photon can also transfer its energy to a loosely bound e- and eject it. Particularly imp. for low Z elements.
- The probability of pure x-ray fluorescence occurring after the initial collision, is ω , the Fluorescence Yield.
- ω depends upon 'Z' and the value of 'n' where the vacancy was created. For a give Z, $\omega_K > \omega_L > \omega_M$
- $\omega \sim 10^{-4}$ for B (Z=5), $\omega \sim 1$ for U (Z=92)
- XRF spectrometry excellent for high Z elements, challenging for low Z



- Fig. 4a: X-ray series. The x-rays are labelled by the shell where the vacancy was created. Lowest energy x-ray of a given (vacancy) shell, is labelled α , subsequently, β , then γ .
- Once a vacancy is created in the K shell a cascade of transitions may ensue leading to the K series, the L series and M series x-rays, depending on the value of Z.
 - Fig. 4b shows such multiple transitions in a medium Z element (Ag)



- The K_{α} transition can be approximated as occurring in a pseudo H atom with nuclear charge $(Z-1)$. Applying the Bohr atomic model,

$$\Delta E = E_2 - E_1 = (-13.6 \text{ eV})(Z - 1)^2 \left(\frac{1}{2^2} - \frac{1}{1^2} \right) = (10.2 \text{ eV})(Z - 1)^2$$

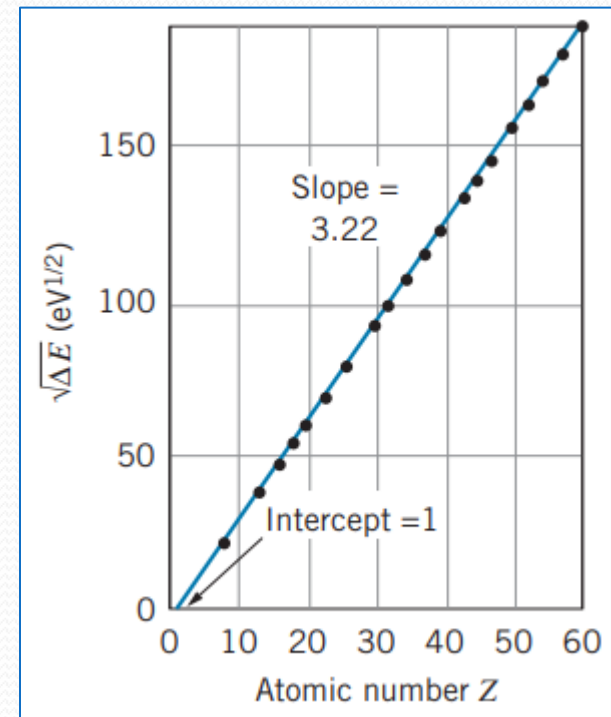
Moseley's Law

E_2 is the energy of the e- in the L shell,

E_1 the energy of the e- in the K shell

- Plot of $(\Delta E)^{1/2}$ vs Z yields a straight line (fig. 5), whose intercept is 1 and slope $(10.2 \text{ eV})^{1/2} = 3.19 (\text{eV})^{1/2}$

which is excellently corroborated by experiment.



- Moseley's law forms the basis of XRF spectrometry: the transition energies carry the imprint of the element's Z

I.4 Interaction of Xrays with matter

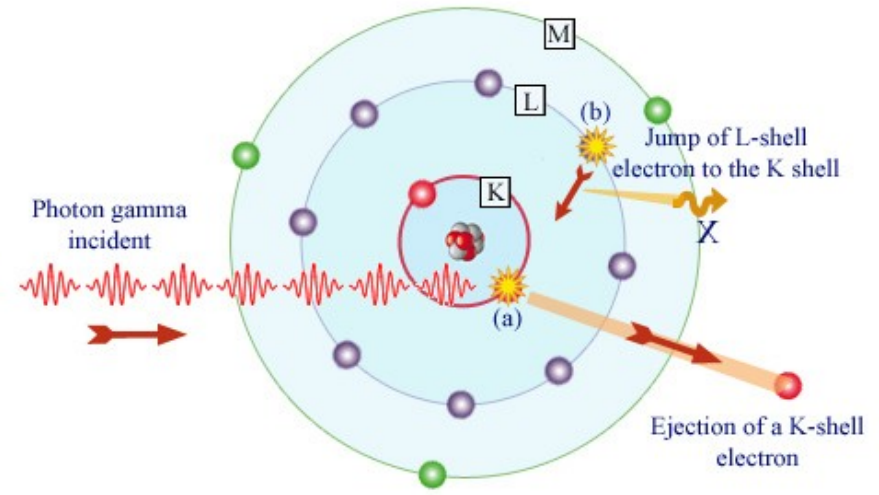
- These interactions are responsible for the observed XRF spectrum
- For an incident radiation energy $< 1022 \text{ keV}$, 3 types of interactions predominate:
 - Photoelectric Effect, Compton (Inelastic) and Rayleigh (Elastic) Scattering

- **Photoelectric Effect:** The x-ray photon with energy, E , greater than the binding energy, B_e , of the atomic electron, gets completely absorbed, resulting in the ejection of the bound e^- into the continuum with kinetic energy, K_e

- $K_e = E - B_e$

- An e^- from an upper shell jumps down to fill the vacancy, releasing the characteristic x-ray.

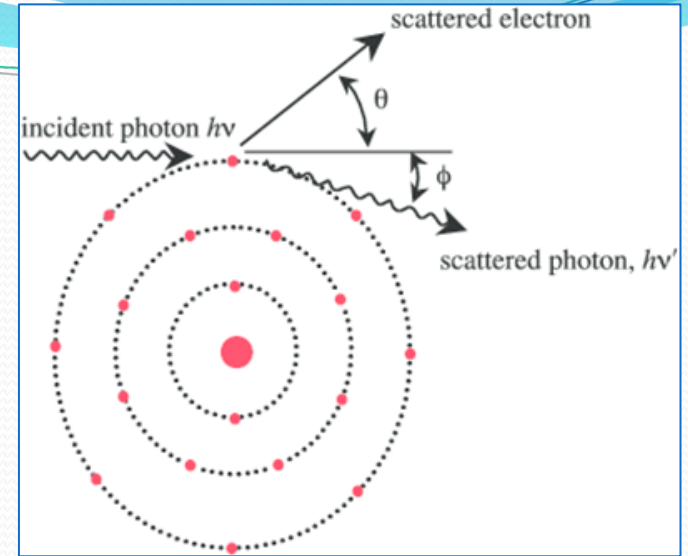
- PE is greater for higher Z elements.
- PE responsible for photopeak in XRF spectrum



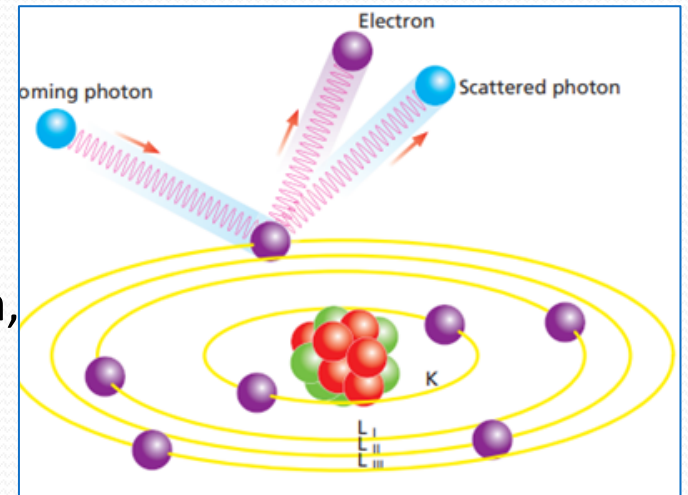
- Compton Scattering:** The x-ray photon inelastically scatters off a loosely bound atomic electron, emerging with energy E' at the angle θ .

$$E' = \frac{E}{1 + \epsilon(1 - \cos \theta)}$$

$\epsilon = E/m_e c^2$;
 m_e is the rest mass of the e-



- Rayleigh Scattering:** Elastic scattering of the photon by a bound e-. The e- oscillates about its orbital position with the same frequency as the incoming photon, emitting radiation of the same incident photon frequency. Appears as 'atomic reflection' of the x-ray.



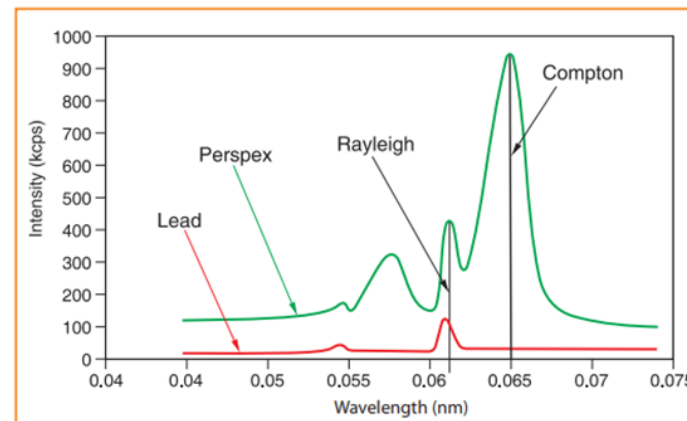
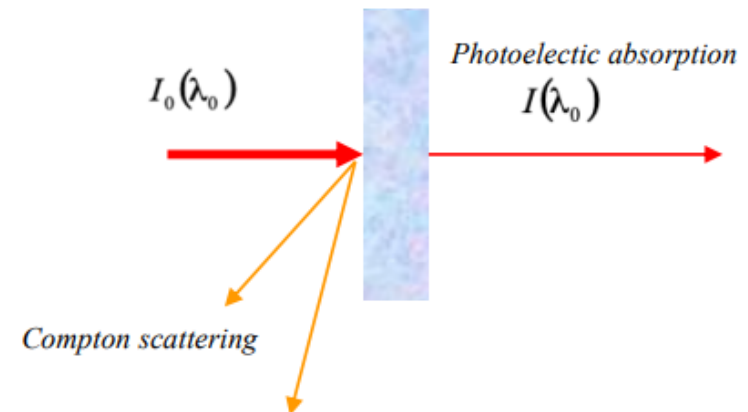
- In PE absorption, only a fraction of the incident beam, of intensity I_0 , gets absorbed the rest is transmitted, with intensity I , according to the **Beer-Lambert Law**:

$$I = I_0 e^{-\mu x}$$

where x is the sample (absorber) thickness and μ_a the attenuation coefficient of the absorber at the incident wavelength/energy.

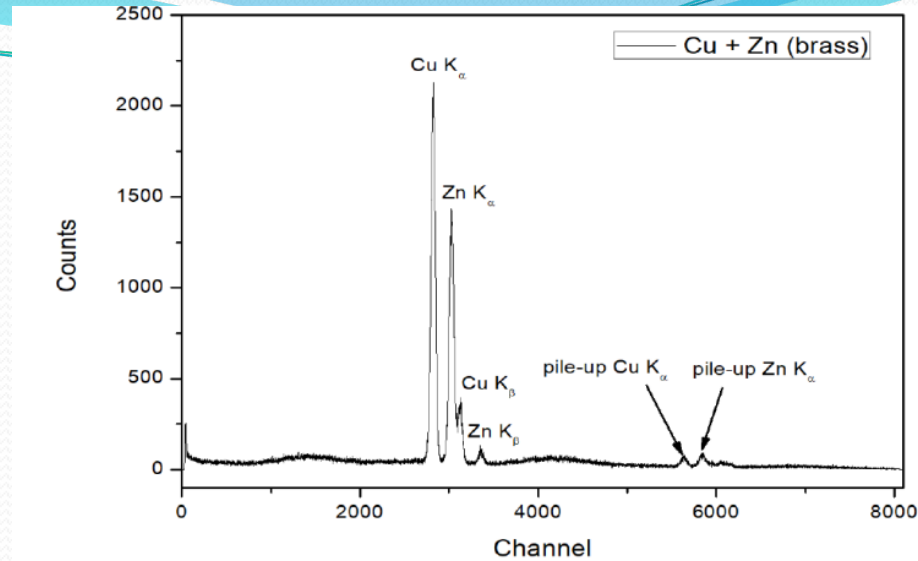
- PE greater for high Z elements, CS for low Z and RS for high Z Elements.

- CS and RS give rise to the background in the XRF spectrum



I.5 XRF spectrum analysis

- The output spectrum:
 - characteristic peaks of the sample,
 - the scattered radiation background continuum,
 - the BR continuum from the x-ray tube together with the characteristic peaks of the anode element,
 - some detector related spectral artifacts of low magnitude such as Escape and Sum (Pile-up) peaks
- The Y axis is in photon counts and the X axis as channel number from the MCA readout
- Spectrum energy calibration: The channel peak positions (after Gaussian fitting) of a standard with known elements is read off as energies using literature data. Multiple identifications used to construct the global energy calibration equation.



- **Qualitative analysis:**

The spectrum of the unknown sample is run and the elements identified from the energies of their peaks (after Gaussian fitting).

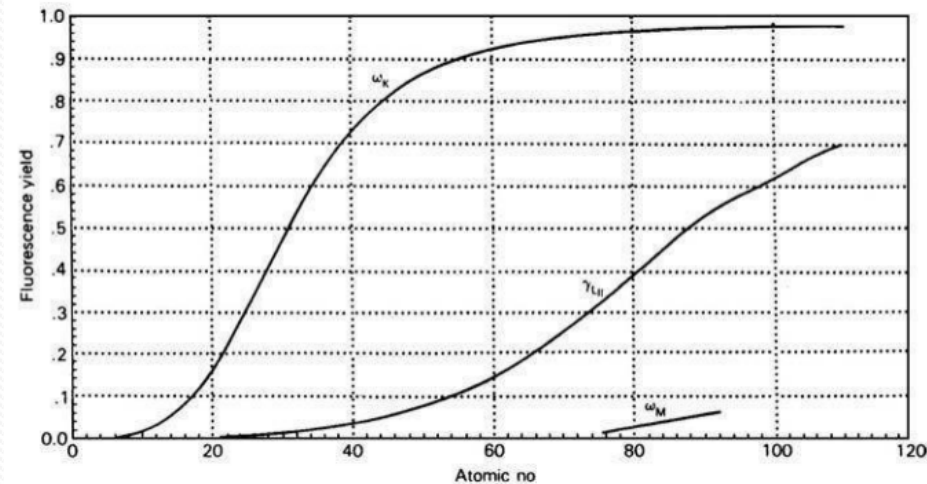
- **Quantitative analysis:**

The integrated peak intensity, (peak area), I , is computed after subtracting the peak background counts from the gross peak area (after Gaussian peak-fit).

Multiplicative corrections for the FY of the transition and the detector sensitivity at the peak energy for the given sample-detector geometry are made to yield the normalized peak intensity, I' .

- The concentration of the i th element, C_i , is

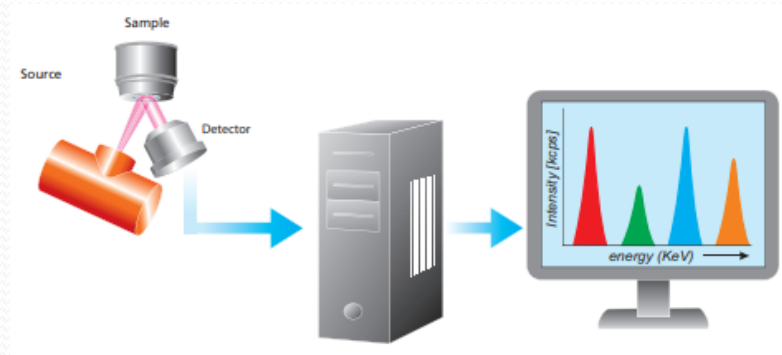
$$C_i = \frac{I'_i}{\sum_i I'_i}$$



where $\sum_i I'_i$ is the sum of the normalized intensities of all involved elements.

I.6 The XRF Spectrometer - Basic and Advanced

- **XRF spectrometer:**
 - a source irradiates the sample,
 - the fluoresced beam is collected and measured by an energy dispersive detector,
 - the signal is analyzed and processed by analog-digital electronics and
 - read-out in discrete channels corresponding to energy bins by a multi-channel analyser.



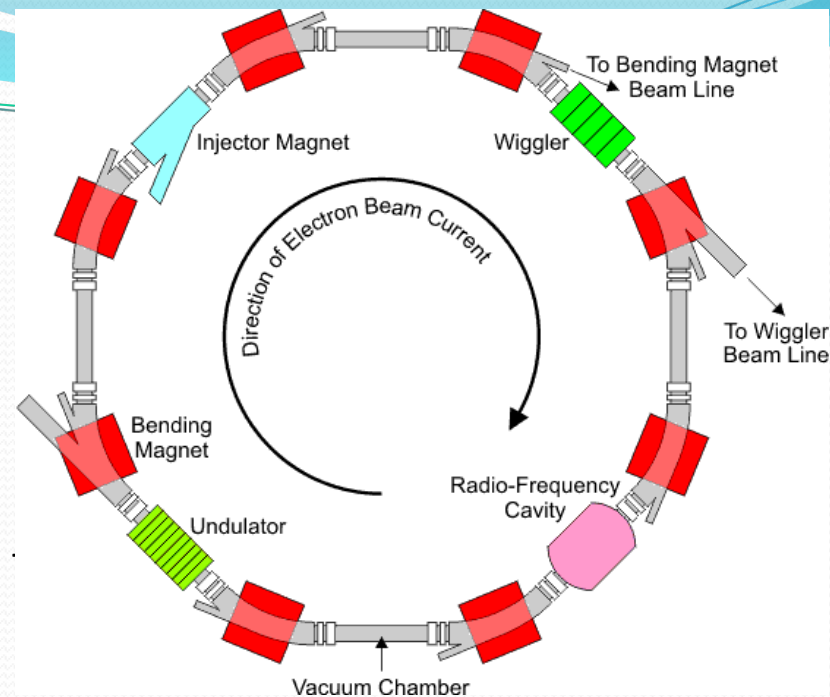
- **Basic XRF spectrometer:**
 - Generally simple source (radioactive or standard tube),
 - 2D optics, => the x-ray path is in one plane.

● **Advanced XRF spectrometer:**

- High performance tube or synchrotron source (sXRF);
- XRF with Total Reflection (TXRF) or Grazing Incidence of the incident beam (GiXRF)
- Microbeam XRF (μ XRF)
- Polarized beam XRF (PEDXRF). XRF with 3D optics => the x-ray path lies in 3d.
- The minimum detection limit (MDL) of tube based TXRF/GiXRF is ~ 10 ppb; sTXRF lowers the MDL to ppt.
- MDL of PEDXRF is ≥ 0.1 ppm
- μ XRF is used for elemental concentration mapping. MDL is \sim hundreds of ppm but much lower for s- μ XRF
- This lecture will focus mainly on TXRF and PEDXRF

The synchrotron

- A synchrotron is a type of circular particle accelerator.
- Accelerates charged particles (electrons) through sequences of magnets until they reach almost the speed of light.
- These fast-moving electrons produce very bright light, called synchrotron light.
- Very intense, predominantly x-ray light, order of 10^6 times brighter than x-ray tube light, order of 10^9 brighter than sunshine.
- Scientists can use this light to study atoms and molecules.
- Synchrotron principle was invented by the USSR scientist Vladimir Veksler in 1944. The first synchrotron was built by the American scientist Edwin McMillan in 1945.
- The initial purpose was to use it as an atom-smasher, to study elementary particles – synchrotron light was considered a “nuisance”.
- Since the 1960s the tremendous potential of synchrotron light to study the atomic and molecular properties of matter was realized. Since then, synchrotrons very largely applied to such studies.
- The “generation” of a synchrotron refers to the technology used to generate the synchrotron light. Currently at generation 3 => special arrays of magnets called insertion devices cause the electrons to wiggle, creating even more intense and tuneable beams of light.



Spectrometry

- The xray path is in 2 mutually orthogonal planes – 3d optics
 - Double reflection about 90°, doubly polarizes the tube radiation, eliminating the scattered background tube radiation
 - Scattered background from the secondary target not completely eliminated because of single 90° reflection.
- Considerable reduction of BR background in the spectrum that greatly improves sensitivity.

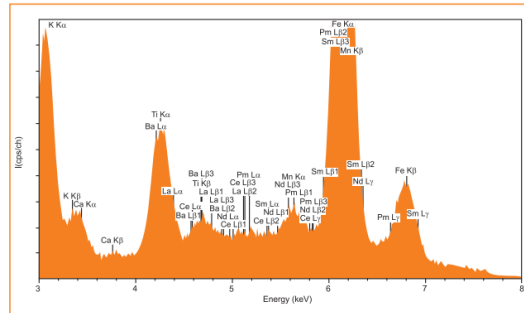
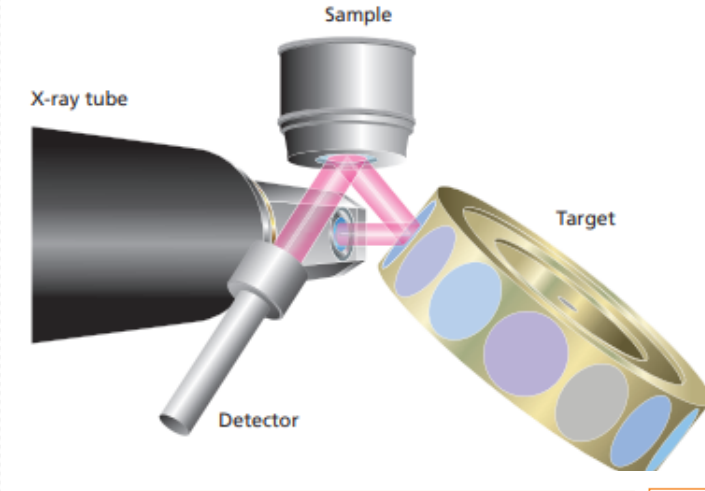


Figure 19. Typical spectrum of a soil sample measured with EDXRF spectrometer having 2D op direct excitation

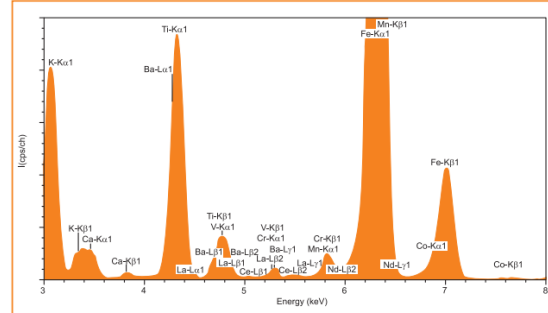
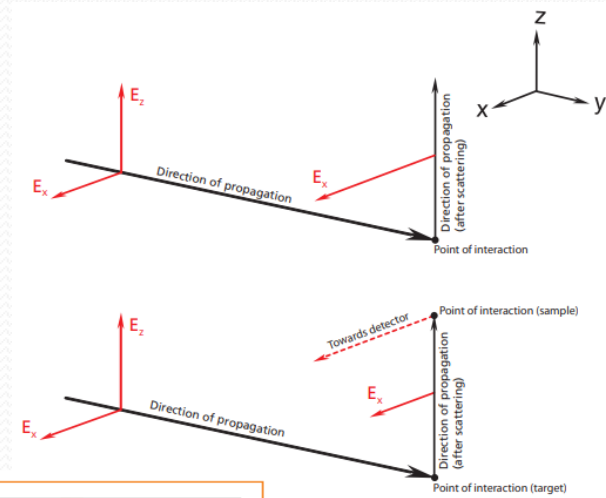
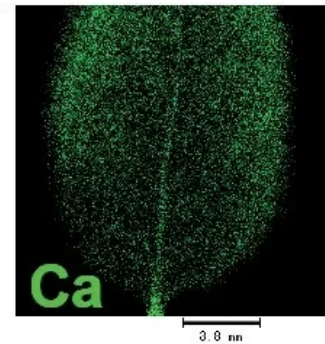
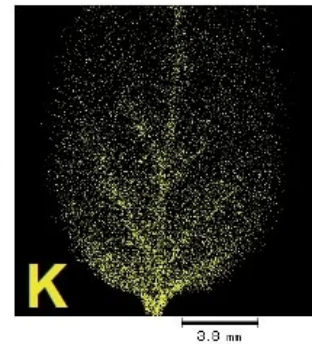
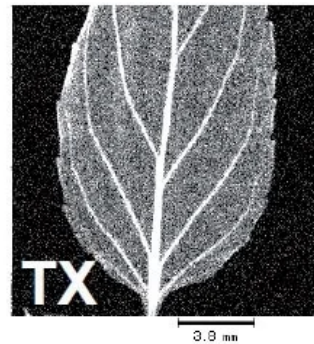
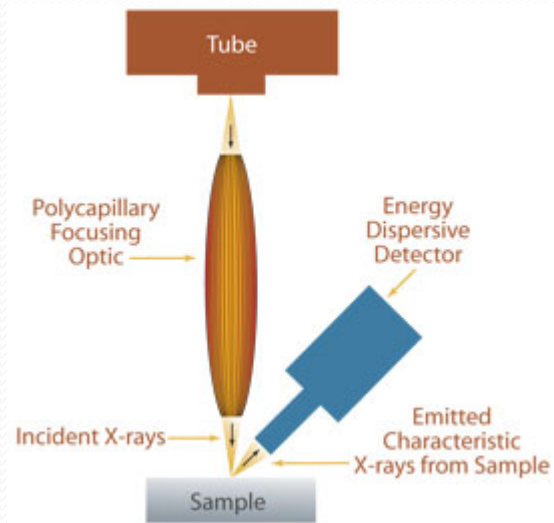


Figure 21. Typical spectrum of a soil sample measured with an EDXRF spectrometer having 3D optics and indirect excitation

Microbeam XRF (μ XRF)

- XRF technique that examines very small sample areas to produce a concentration map of the surface
- Polycapillary and doubly curved crystal focusing optics collect x-rays from the divergent x-ray source and direct them to a small focused beam at the sample surface with diameters as small as tens of micrometers.



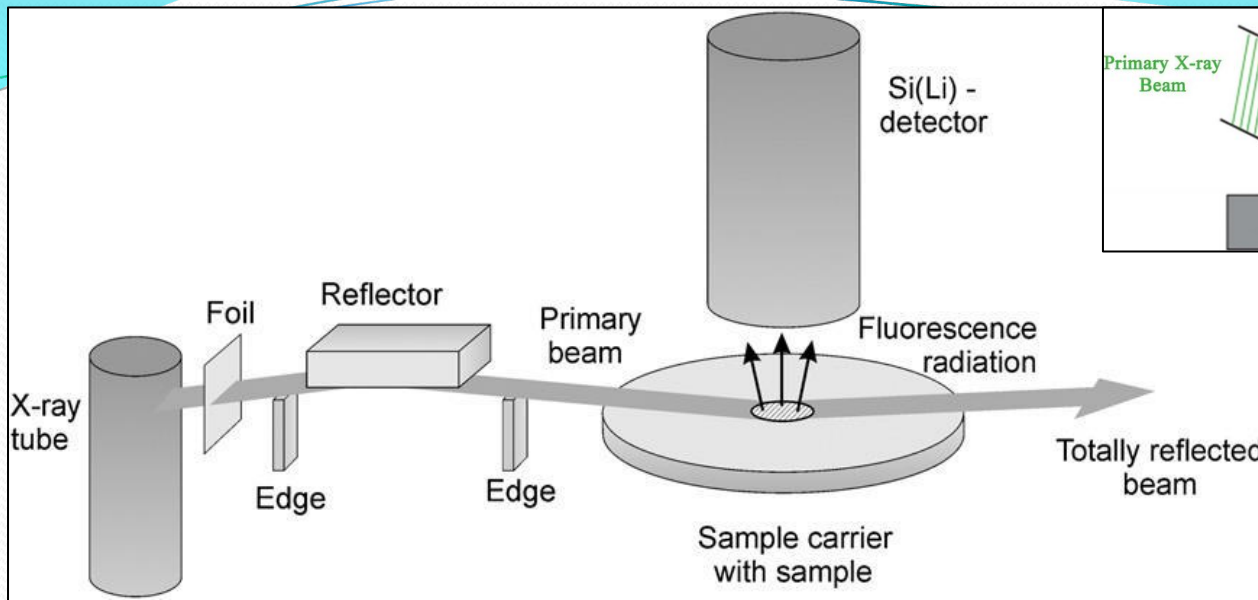


Fig. 3.1 Layout of the TXRF system

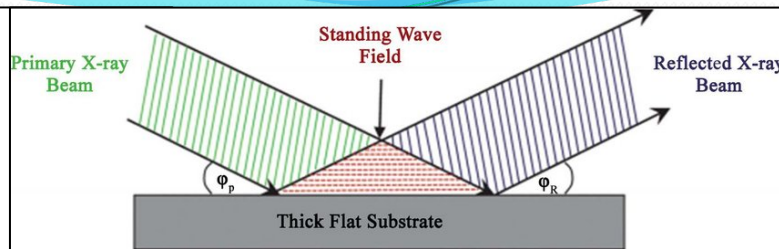


Fig. 3.3 X-ray Standing Wave

This work:

- Bruker S2 Picofox TXRF system (air ambient)
- FOMs using Bruker's SPECTRA-7[®] analysis software
- Matrix effects using ORIGIN 9.1 and linear background fit to the peaks

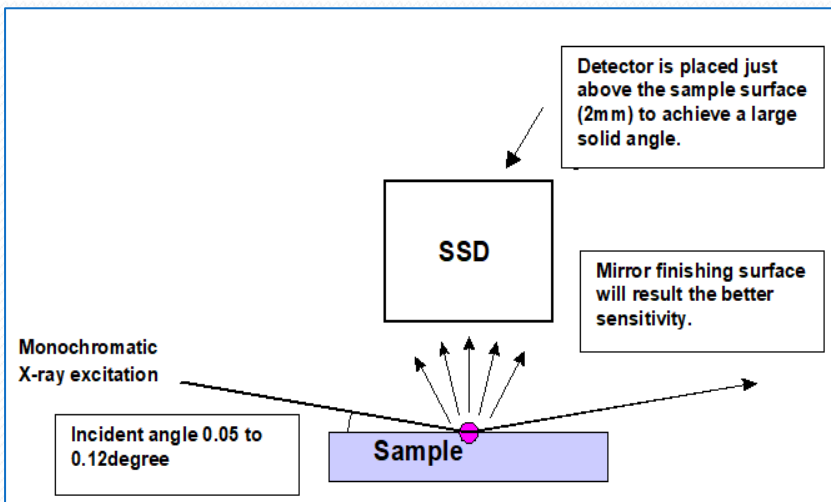


Fig. 3.2 Principle of total reflection on a highly polished substrate disc containing the sample

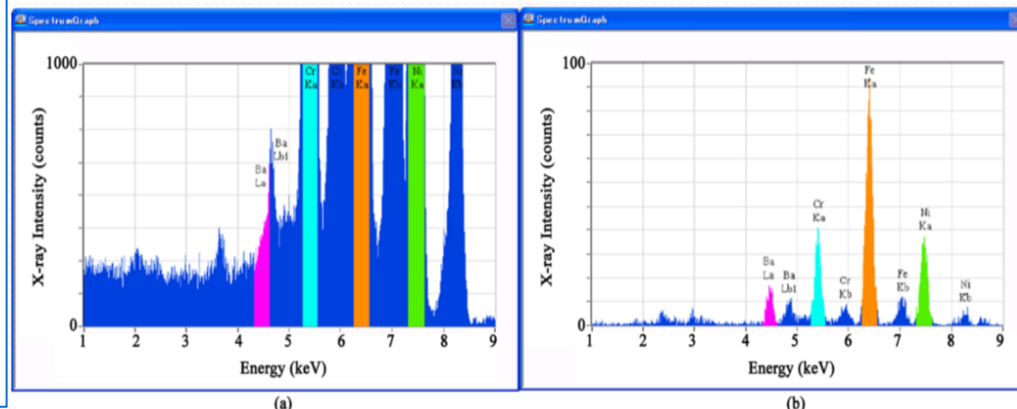


Fig. 3.4 XRF (left) and TXRF (right) spectra. Higher S/N and therefore higher sensitivity in TXRF



II. Applications

- Examples of applications from the research carried out in the Laboratory of Biophysical Chemistry and Radiation Studies (LBER) at the University of Michoacan, Morelia, Mexico.
- Areas of research touch upon,
 - Volcanic geochemistry
 - Biomedical elemental analysis
 - Environmental pollution analysis
- Techniques used:
 - PEDXRF
 - TXRF

Heavy Elements of the 5th to 7th Periods in the Fumarolic Microecology of the Los Azufres (Mexico) Volcanic Complex: Clues to Deep-Earth Radioactivity?



Nabanita Dasgupta-Schubert

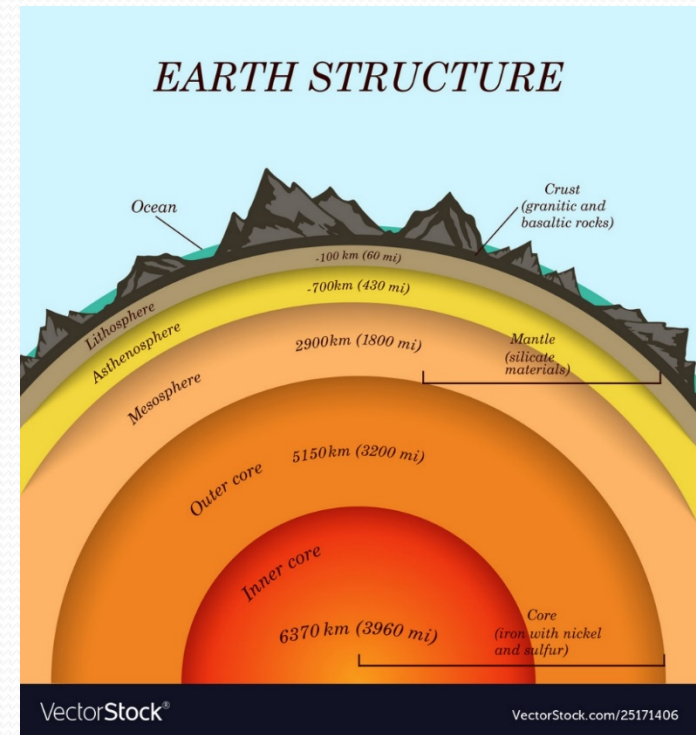
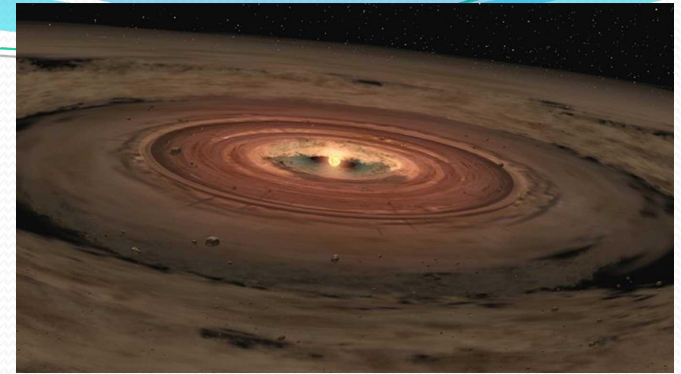
Department of Physics and Mathematics
University of Michoacan, Morelia, Mexico



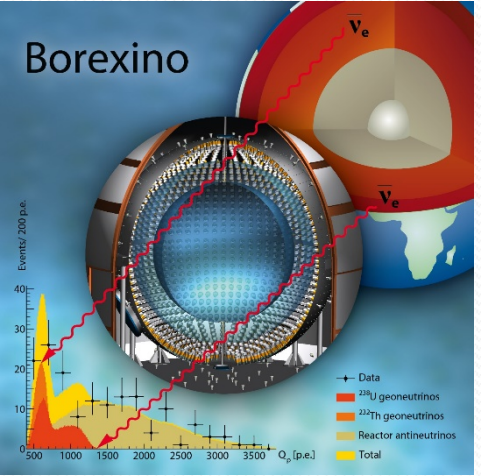
**XLV Symposium on Nuclear Physics
Cocoyoc, Morelos, México.**

The Earth's Interior

- **Formation of the Earth:** Over 4.6 billion years ago. Gradual accretion of dust and gases around the young sun.
- **Structure of the Earth:** 3 principal layers – Crust, Mantle and Core.
- **The Mantle:**
 - 87% of the Earth's volume; 67% of its mass. Solid but behaves like a viscous fluid.
 - Responsible for Earth's bulk composition, volcanism, earthquakes, introduction of vital elements to the crust.
 - Composition: Mostly silicates of Mg, Fe, Al, Ca, Na, K. Information on minor and trace heavy elements (HE) is scant.
 - Minor and trace elements in dissolved phase and carried up to the crust by geothermal fluids.
 - Chemical composition determined from deep bore-hole extracts, chondritic meteors, volcanic rocks

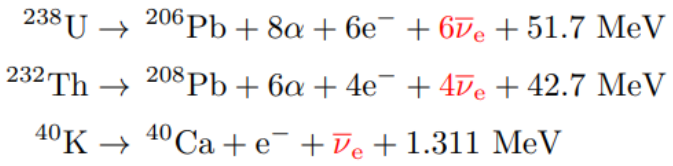


Two recent discoveries that highlight the need to know the Mantle's elemental composition and its distribution: (a) The Borexino (PRD, 2020), KamLand (Geophys.Res. Lett. 2022) geoneutrino determinations (b) The localization of Theia (Nature, 2023).

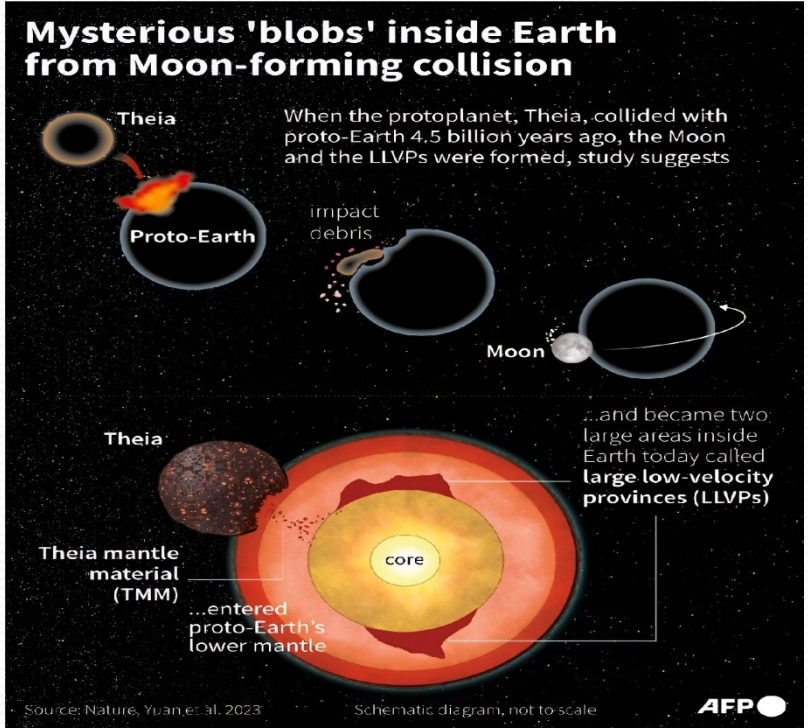


Radiogenic heat (RH):
 $H_{\text{rad}}(\text{U}+\text{Th}+\text{K}) = 32.8^{+13.6}_{-12.7} \text{ TW} \sim 50\%$ of the total heat generated by the Earth.
 The rest is the primordial heat and other (unknown) sources.

Emission of $\bar{\nu}_e$ from U, Th and K.



The U, Th, K concentrations were obtained from chondritic meteors



2 continental sized blobs in the Mantle, below the Pacific and Africa that are the remnants of Theia.

These blobs are denser, more HE rich, than the Mantle. Likely alter Mantle's localized elemental composition.

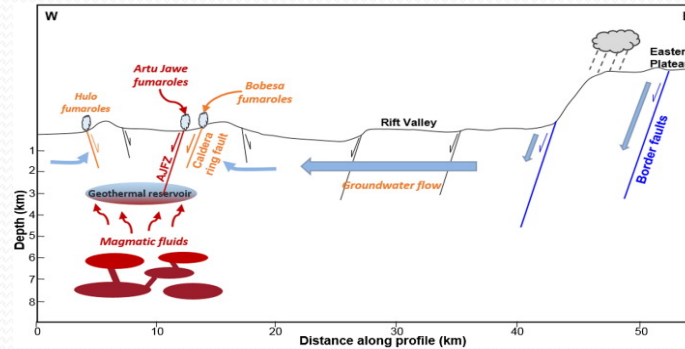
Need to obtain accurate estimates of the concentrations of U, Th, K (and other elements) in the Mantle as well as their geographical distributions.

Fumarolic vapours as proxy for direct Mantle sampling.

Fumarolic mosses as element collectors

What is a fumarole?

- Fumarolic vapour generally collected by piping it into an evacuated chamber.



- Special precautionary techniques required because of the acidity, toxicity, T of the fumarolic vapours; possible secondary elemental contamination.

Our idea:

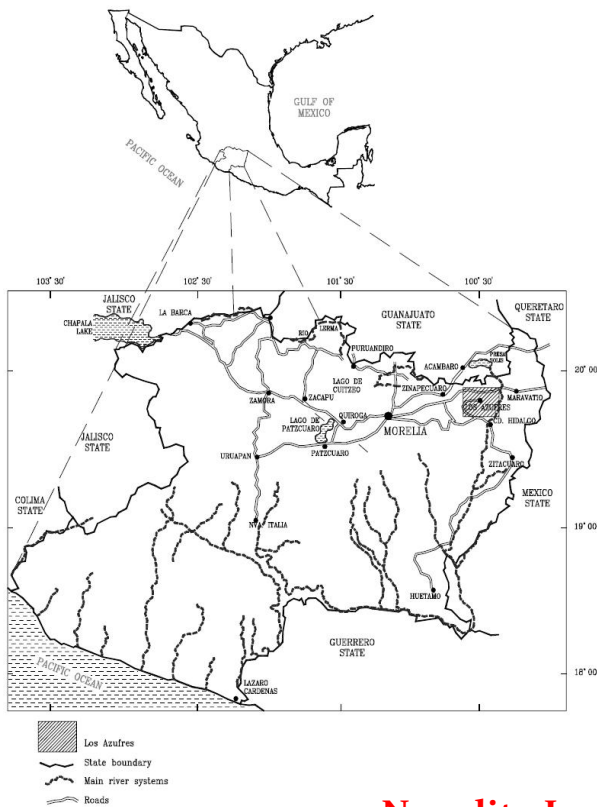
- To use the primitive extremophilic plants - largely mosses - that ring the fumarolic mouths, as collectors of the elements of the fumarolic vapours.
- These plants have High T and toxic/acidic vapour tolerance.
- The plant's tissue maintains a repository/template of the fumarolic elemental composition by direct absorption and storage of nearly all the HE from the fumarolic vapours.



- XRF spectrometry (XRFS) - widely used technique for the simultaneous & non-destructive analysis of elements, principally from Na to U.
- Traditional XRFS - relatively low sensitivity (low S/N) because of Bremsstrahlung background and matrix effects => non-trace analysis only.
- Recently, several notable technological advances coupled with improved spectrum Fundamental Parameter analysis algorithms, e.g. polarized energy dispersive XRFS (PEDXRFS) and total reflectance XRFS (TXRFS), allow high sensitivity => trace and ultra-trace elemental analysis
- This work - PEDXRFS with FP algorithm applied to elemental analysis of the components of the Los Azufres geothermic microecology comprised of the plants (mosses (M) and ferns (F)) and rhizospheric soils of the fumaroles (RS), the hot-spring sediments (S) and the native volcanic substrate (VS)

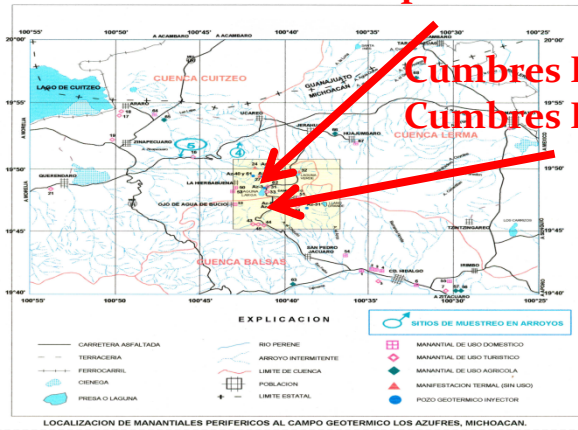
The Los Azufres Geothermal Complex

- Located 220 km WNW of Mexico City. Altitude of 2000-3000 m. Covers an area of $\sim 40 \text{ km}^2$
- Zones investigated in this work are the nearly completely anthropogenically undisturbed sites of Nopalitos (NOP), Cumbres I (CI) and Cumbres II (CII).
- Avg, O_2 level at 74% of sea level, avg, precipitation 14 times higher than global average.
- These sites characterised by fumaroles and hydrothermal springs



Nopalito I

Cumbres I & Cumbres II



Los Azufres fumarolic and hydrothermal microcosm

Physicochemical properties of the fumaroles and hot springs (Abuhani et al, 2015 J Env Rad)

- Fumarole:

Air Temperature: 45°C (NOP), > 45°C (CI, CII).

Gas conc. (% of total GV): Steam 97.4, Non-condensable gases (NCG) 2.6

NCG gas conc. (% of total NCG): CO₂ 97.4, H₂S 2.3, O₂ 0.2, Other gases 0.1

- Hot-spring:

Water temperature range 80°C (NOP) – 88°C (C2)

pH range 1.95 (C1) -2.31 (NOP)

Electrical conductivity (μS/cm), 3770 (NOP)- 6580 (C1)

Max. Conc. (mg/L) of dissolved ions and neutral species:

Cl⁻ 52.7 (C2) | (SO₄)²⁻ 4472 (C1) | (HCO₃)⁻ 0 | SiO₂ 456 (C1)

Extreme conditions that mirror conditions on paleo Earth.

Only extremophiles thrive in this ecological microcosm:

Primitive bryophytic and pteridophytic plants

e.g. mosses and ferns, and archaic bacteria.



Mirrors the landscape of earth in the Ordovician – Devonian

periods hundreds of million years ago when these were the first plants to colonize land.

WAA, NDS et al, 2015; WAA, NDS et al 2019(a); WAA, NDS et al 2019(b); WAA, NDS et al 2021

Objective and outline of this work:

- Los Azufres geothermal microcosms taken as natural repository of HE exuded from the Earth's upper mantle via fumarolic vapours, hot-springs and the residual volcanic substrate .
- We have investigated the fractionation of elements of the 3rd to the 7th period between the plant tissue, the rhizospheric soil, the pure volcanic substrate and the hydrothermal sediments (designated the ecological components)
- To observe the degree of dispersion of the HE concentrations over time and at different locations within the Los Azufres volcanic complex.
- To compare the grand averages of the concentrations of the HE between the different ecological components with the few published data that exist on HEs of fumarolic gases and with the estimates of the Mantle's concentrations.
- To try to understand the source of the HE mass distributions in the fumarolic vapours of Los Azufres

Presented here are the results of Cd, Hg, Pb, Th, U - 5 of the heaviest naturally occurring metals for all the components and later the concentration average of all the components for 16 HE of $Z = 30 - 92$.

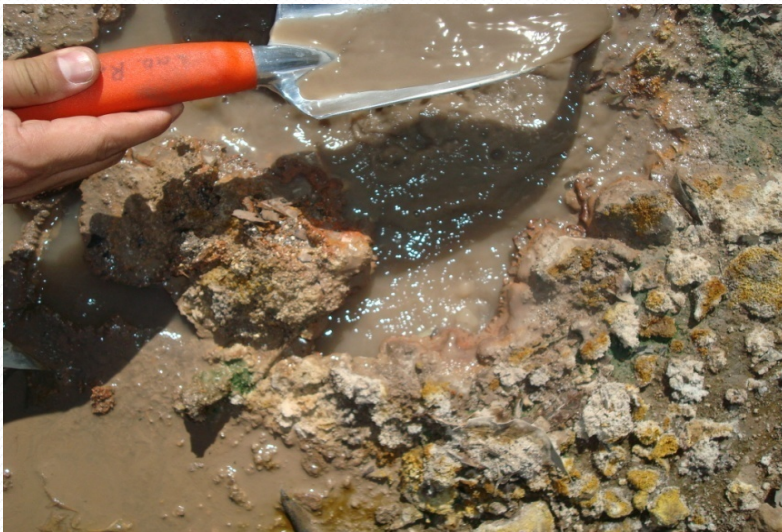


Experimental Part 1: Sample Collection

- Sediment and water collection



Nopalito



Cumbres 1



Cumbres 2



Experimental Part 1: Sample Collection

- Plant, rhizospheric soil and volcanic substrate collection



Nopalito , soil near rocks –
pure volcanic substrate



Cumbres 2 showing Club Moss (grows only in
geothermal regions).



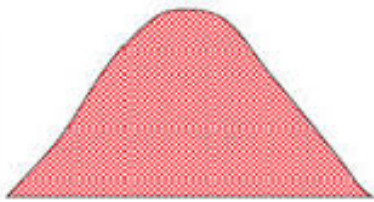
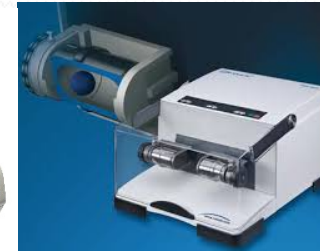
Nopalitos, fumaroles





Specimen preparation Polarised Energy Dispersive Xray Fluorescence (PEDXRF) spectrometry

- Plant and soil samples washed, dried at 60°C for ≥4 d. Sediment and water separated by decanting then by centrifugation.
- Solid samples ball milled 10 min @ 25Hz then sieved for particle sizes <100 μm
- Samples pelletized by a hydraulic press @ 10.4 tonnes



4 g Powder



Pellet

Pellet diameter 25 mm



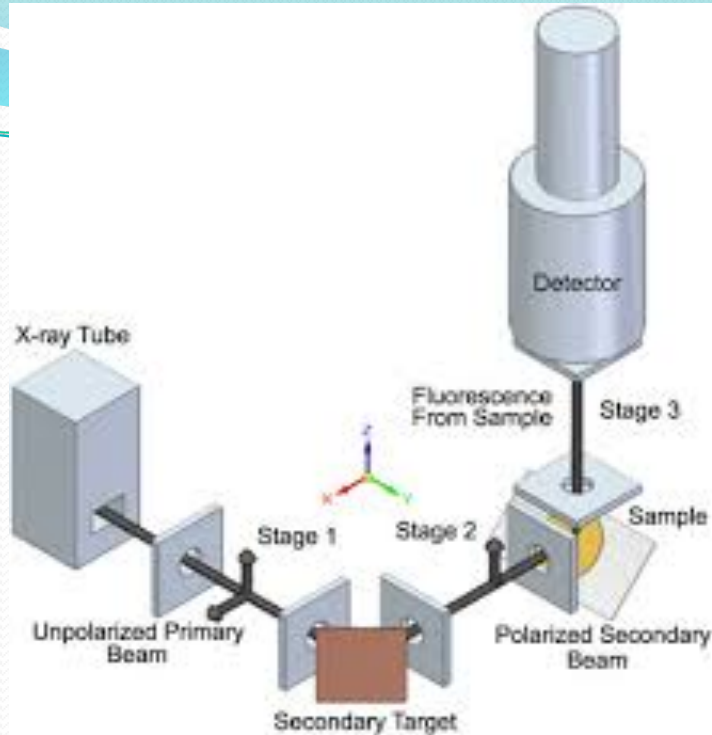
- Pellets were loaded onto the sample holders (cups) and x-ray window was sealed with a Prolene film (4 μm)

- Altogether 33 Plants representing > 30 species, 6 Rhizospheric soils (RS), 6 hot spring Sediments (S), 4 water samples and 1 pure Volcanic Substrate (VS) were sampled with statistical replication

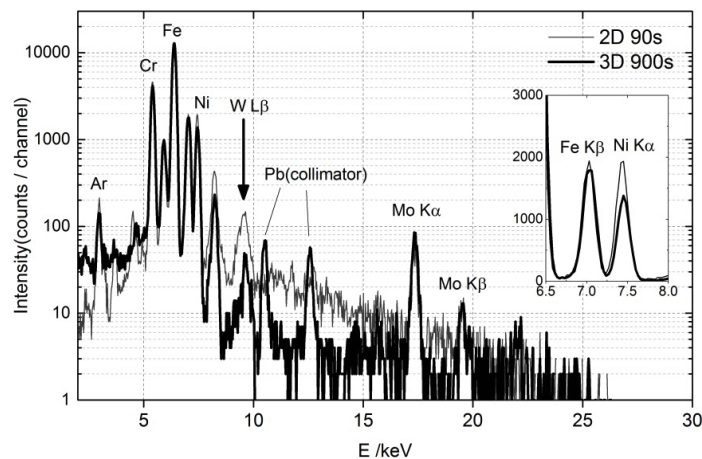


PEDXRF analysis

- Double orthogonal optics cancels out the Bremsstrahlung background from of the primary x-ray source. High sensitivity (parts per million level) and accuracy achieved. (*Abuhani et al, 2015 Powder Diffr. 29: 159-169*)
- SpectroXepos III spectrometer. 50 KV Xray tube, 1 μ A current. 8 secondary and polarization targets (HOPG Bragg crystal, Al₂O₃ Barkla scatterer, Mo secondary target) 30 mm² Peltier cooled Si Drift Detector resolution <155 ev at 5.9 keV. He atmosphere. Na-U analyzed in a single run.
- Quantitative analysis by standardless Fundamental Parameter method using the code TURBOQUANT. Calculates elemental concentrations using built-in theoretical libraries for each matrix type (pellet, powder or liquid). Thus, matrix effects are taken into account



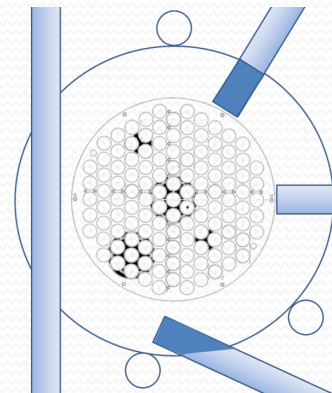
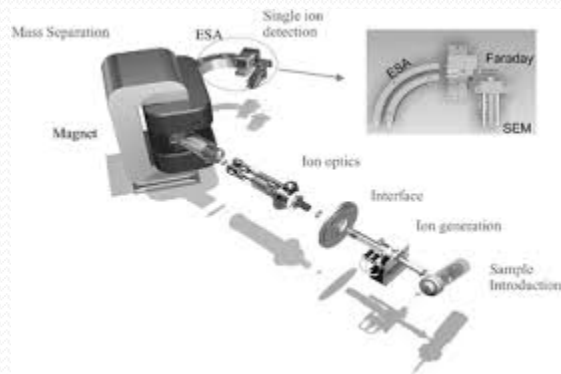
PEDXRF spectrometer with double polarization



Spectrum of ASTM 316L. 25KV tube, 1 μ A with early 3D optics showing background reduction

Inductively Coupled Plasma sector field Mass Spectrometry (ICP-sfMS) and Neutron Activation Analysis (NAA)

- Cross validation of the PEDXRF method was carried out by the simultaneous analysis of constructed multielemental plant secondary standards by ICP-sfMS (Element XR, Thermo Fisher Scientific, Waltham, MA, USA). carried out at the Helmholtz Centre for Environmental Research, Leipzig, Germany. The dry plant matter was digested and analysed at 1:20 dilution by ICPsfMS



- Th and U contents of the fumarolic samples were cross validated by NAA carried out at the Mark II Triga Reactor of the Univ. of Texas at Austin, USA

Table 2a: Average ($n \geq 3$) elemental concentrations of the volcanic substrates VS collected at the sites of N₁ and C₂, and the average concentration in the Earth's crust (from WebElements). Z is the element's atomic number. Gr.Avg: grand average, * estimated concentration

Element	Z	Elemental mass fractions (mg/kg)			
		Earth's crust	VS(N ₁)	VS(C ₂)*	Gr. Avg. VS
Cd	48	0.150	1.20±1.13	1.01	1.10±0.14
Hg	80	0.067	12.85±0.92	14.13	13.49± 0.90
Pb	82	10.00	18.40±3.25	34.11	26.26±11.11
Th	90	6.00	8.35±0.35	17.37	12.86± 6.38
U	92	1.80	0.13±0.002	0.52	0.33± 0.28

Table 2b: Average ($n \geq 3$) elemental concentrations of the rhizospheric soil (RS) and the hot-spring sediment (S) samples.

Element	RS(N ₁)	RS(C ₂)	Gr.Avg. RS	S(N ₁)	S(C ₂)	Gr.Avg. S
Cd	1.93±0.11	1.34±0.48	1.63±0.42	2.0	1.5	1.75
Hg	9.40±3.68	23.89±22.89	16.64±10.24	5.98±2.16	18.83±3.85	12.40±9.09
Pb	13.18±1.45	28.55±5.69	20.86±10.87	14.13±0.39	21.95±0.85	18.04±5.53
Th	6.08±0.25	11.75±3.55	9.86±4.02	5.95±0.28	12.55±2.05	9.25±3.99
U	0.15±0.02	0.81±0.39	0.60±0.44	0.21±0.02	1.17±1.06	0.69±0.83

Table 2c: Average ($n \geq 3$) elemental concentrations of the plant samples at the N₁ and C₂ sites. M = moss; F = Fern.

Element	Plant(M)	Plant(F)	Gr.Avg. Plant	Ordinary modern Plants
Cd	1.81±0.40	1.16±0.51	1.5±0.45	0.025
Hg	2.15±0.28	1.53±0.11	1.84±0.31	0.06
Pb	23.72±0.55	15.79±0.47	19.76±4.0	20
Th	1.89±0.12	0.97±0.19	1.43±0.46	0.03-0.3
U	0.69±0.15	0.73±0.13	0.71±0.02	0.07-0.2

- The rhizospheric soil (RS) concentrates almost all the heavy metals to values higher than the native volcanic substrate (VS) and at levels that exceed the global average crustal rock concentrations.
- The extremophile plants absorb much larger concentrations of the heavy metals compared to ordinary plants, because of their underlying substrate and because of their physiology. Mosses are more effective than ferns. *Bears out our initial hypothesis of using fumarolic mosses as repositories of HE brought up from the Mantle.*
- RS heavy metal concentrations are slightly higher than the sediment concentrations. High temperatures, high ionic/particulate concentrations of hydrothermal waters may dissolve out/colloidally adsorb more of the heavy metal, leaving the sediment poorer.
- Taken together, RS + Plants, sequester more heavy metals per mass than sediments despite the aggressive chemistry of the hydrothermal environment. Remarkable given their non-voluminous root structure.
- Implies that biogeochemical processes play a pivotal role in the capture, distribution and recycling of heavy metals.
- For all geothermal components (P, RS, S, VS) there was more variation with location than with time, indicating that the underlying magma and its associated geochemical processes are not homogeneous.

Comparison of the Grand Average of the HE concentrations over all geothermal components (plants, RS, S, VS) of this work with the estimated concentrations in the Primitive Mantle (Crust+Mantle) of Lyubetskaya and Korenaga *J. Geophys. Res.* 2007 and with the concentrations of fumarolic HE collected in the fumarolic S deposits of the Ebeko volcano, Kurile Is. Shevko et al, *Geofluids*, 2018.

Element	Z	At. Weight	Concentration (mg/kg)		
			This work	L&K	Shevko
Zn	30	65.4	47.94±1.92	0.06	13
As	33	74.9	5.05±1.41	0.05	5.1
Cd	48	112.4	1.50±0.33	0.05	0.18
Sn	50	118.7	20.00±0.08	0.10	0.56
Sb	51	121.8	10.15±4.01	0.01	0.15
Cs	55	132.9	5.92±1.77	0.02	-
Ba	56	137.3	178.69±145.27	5.08	-
Hf	72	178.5	2.83±2.85	0.23	-
Ta	73	181.0	1.75±0.31	0.03	-
W	74	183.8	1.04±0.12	0.01	-
Hg	80	200.6	7.58±9.95	0.01	-
Tl	81	204.4	0.88±0.04	0.002	-
Pb	82	207.2	20.98±4.50	0.14	5.3
Bi	83	209.0	0.94±0.06	0.004	-
Th	90	232.0	4.24±4.89	0.06	1.3
U	92	238.0	0.83±0.20	0.02	0.95
Th/U			5.12	3.65	1.37

Summary and Conclusions

- We have shown that the biogeochemical microecological niche of fumaroles with its extremophilic plants acts as an efficient and inert absorber of the HE from the fumarolic vapours.
- We have proposed that this property can be leveraged to proxy the Mantle's HE composition. Suitable accounting of the selective geochemical loading of the HE in the fumarolic vapours in the Mantle, becomes necessary.
- We have used the sensitive and high-throughput nuclear analytical technique of PEDXRFs to make a detailed assay the HE concentrations of the fumarolic microecology of the Los Azufres volcanic complex.
- We show that considerable discrepancies in the known HE composition of the Mantle exist. Our determinations lie on the higher side of indirect estimates made from meteoric/volcanic rocks.
- Need for many Mantle HE composition determinations throughout the world, to ascertain the extent of HE inhomogeneity in the Mantle and determine its source (Theia?)
- The Th/U ratio which enters into the calculations of the Earth's internal heat (Borexino and Kamland experiments) is demonstrated to be quite variable. Our value is on the higher side.



UNIVERSIDAD MICHOCANA
DE SAN NICOLÁS DE HIDALGO

Analytical characterization of the bench-top TXRF spectrometric assay of Selenium in a complex matrix.

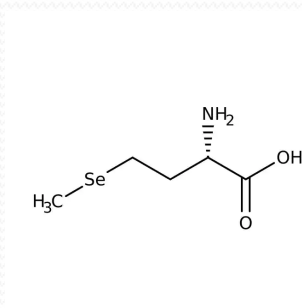
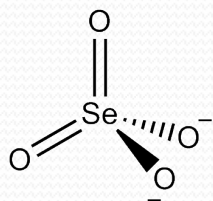
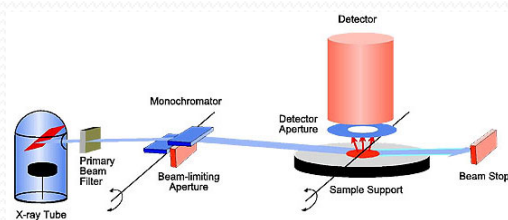
Nabanita Dasgupta-Schubert

Department of Physics and Mathematics
University of Michoacan, Morelia, Mexico



The preamble....

- We discuss the relatively new form of bench-top analytical X-ray spectrometry that uses the property of the total reflection of a grazing X-ray beam on a perfectly reflective sample-containing substrate, to achieve analytical sensitivities of \leq ppb (parts per billion) and line-shape parameters that permit the possible identification of Chemical Shift (molecular environment) effects, in the energy dispersive mode of X-ray fluorescence spectrometry (XRFS)



- Se in simple (Selenate ion) and complex (amino acid dl-Selenometionine) molecular forms.

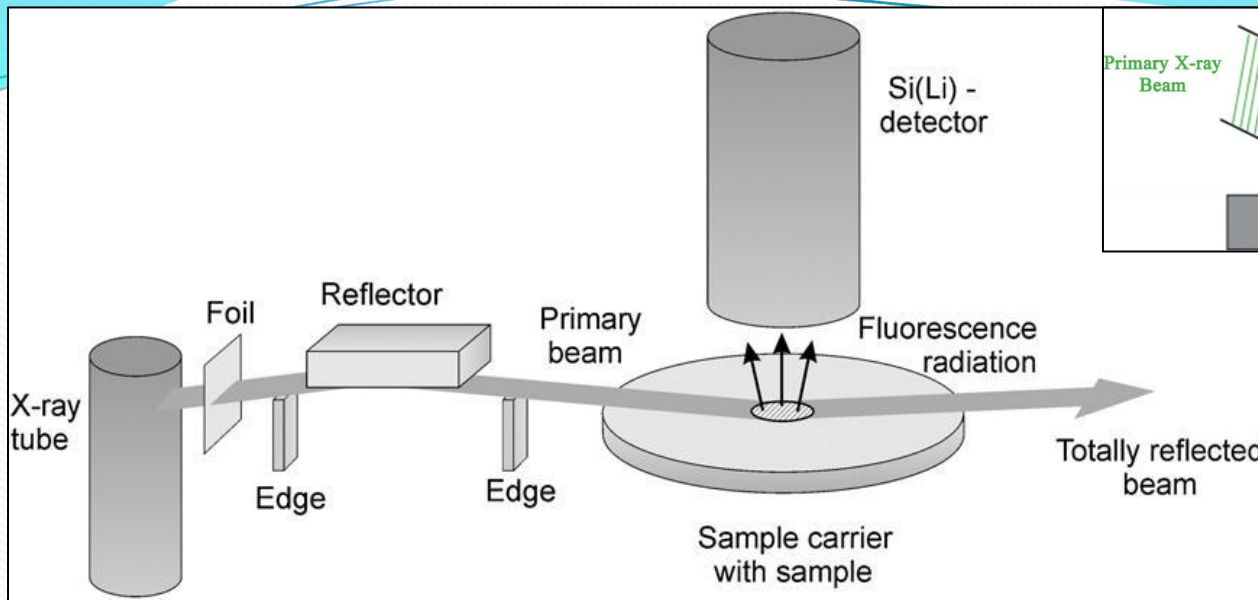


Fig. 3.1 Layout of the TXRF system

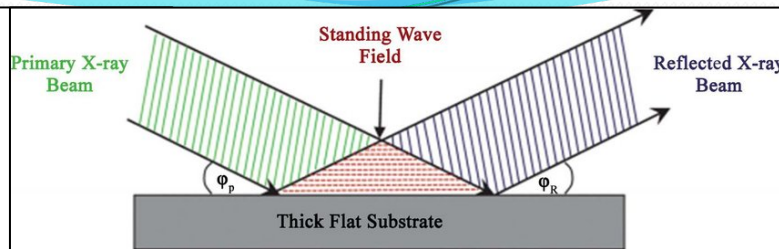


Fig. 3.3 X-ray Standing Wave

This work:

- Bruker S2 Picofox TXRF system (air ambient)
- FOMs using Bruker's SPECTRA-7[®] analysis software
- Matrix effects using ORIGIN 9.1 and linear background fit to the peaks

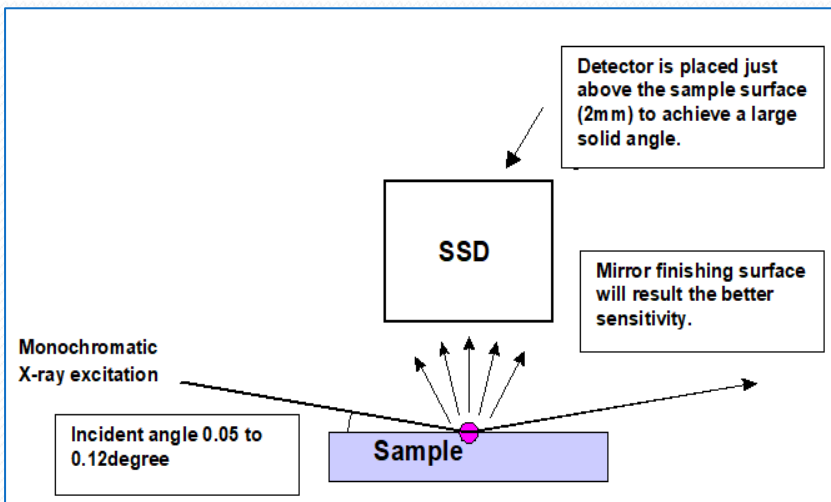


Fig. 3.2 Principle of total reflection on a highly polished substrate disc containing the sample

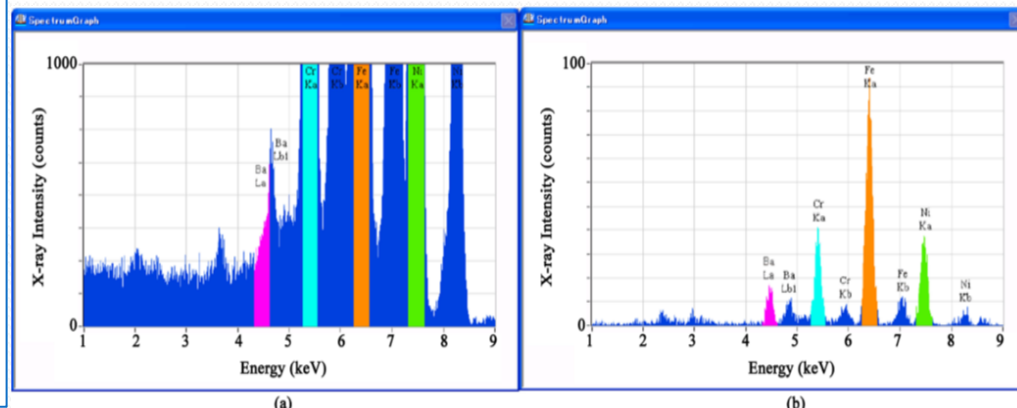
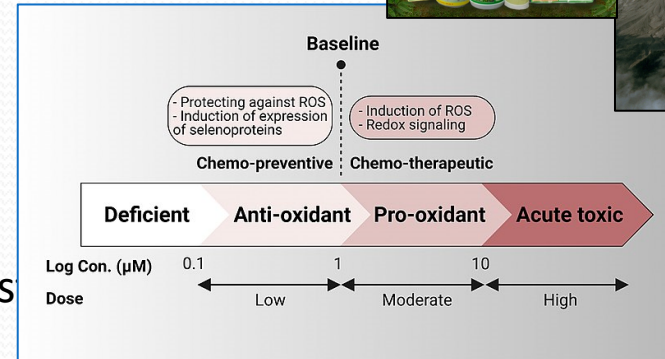


Fig. 3.4 XRF (left) and TXRF (right) spectra. Higher S/N and therefore higher sensitivity in TXRF

Selenium (Se) and the Elemental Analysis of Se

- Se: a metalloid, Z = 34, Group 16 (O-S-Se-Te-Po-Lv)
- Environmental sources: Volcanic emissions, agricultural chemicals, industrial waste etc.
- Biological utility: An essential micronutrient.
Toxic at high concentrations – selenosis;
Deficiency – Keshan's disease.
Tolerance range is narrow.
- Implicated in DM Type 2. May confer Covid resis



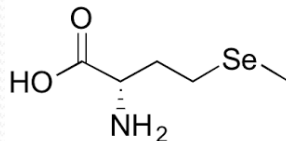
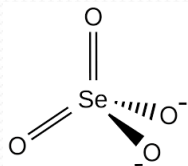
- Accurate, Precise, Highly Sensitive Quantitative Analysis of Se in complex matrices - essential components of the **Figures of Merit (FOM)** of elemental atomic analysis.
- A large linear dynamic range – ppb to fractions of % so that samples of all provenance can be analyzed by one technique.

Total Reflection X-ray Fluorescence Spectrometry (TXRFS): Relatively recent technique. Result of continual advancement of R&D in x-ray instrumentation and applications. Proving to be attractive for the elemental analysis of a wide range of materials including nuclear materials.

OBJECTIVE of this work: Validate the quantitative analysis of Se metabolites in simulated human urine (a complex matrix) using TXRFS through a detailed examination of FOMs and Matrix Effects. What can be learnt from these?

Selenium metabolites in human urine, Composition of artificial human urine (AHU) and Sample preparation

- Urine main excretory route of Se
- Typical metabolites: Selenate(SeT) and dl-Selenomethionine (SeMet)



- Natural HU unsuitable for validation studies because of wide variability
- Composition of AHU (modified from Khan et al 2017 doi:10.1128/jmbe.v18i2.1325):
 - KCl, 0.2 g/l
 - NaCl, 8 g/l
 - Na₂HPO₄, 1.14 g/l
 - KH₂PO₄, 0.2 g/l
 - Urea, 9.3 g/l
- **Solutions of SeT and SeMet prepared @ 0.01-100 mg/l in tri-distilled water (t-DI) and AHU @ pH 7 (except for SeT in t-DI @ pH 1)**
- All reagents were AR grade



Fig. 4.1

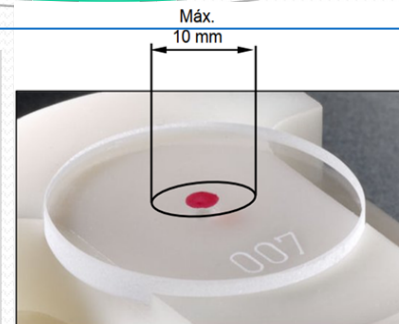


Fig. 4.2



Fig. 4.3

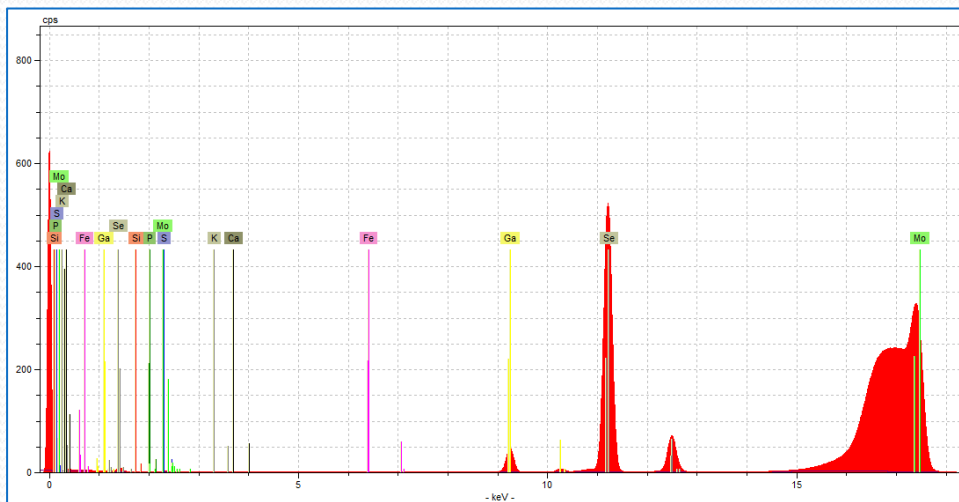
- Samples: Se solutions spiked with Ga as internal standard @ 0.1 – 10 mg/l
- 10µl of sample aliquoted onto 30 mm previously hydrophobized acrylic discs (fig. 4.1) on the disc centre, with dia ≤ 10 mm (fig. 4.2)
- Sample discs oven-dried slowly @ 35°C for 30-40 mins, to prevent SeMet volatilization. Dried sample measured ~ 0.52 mm dia (fig. 4.3)



Fig. 4.4

The 100 mg/l SeT sample in AHU was highly hygroscopic, hence discarded

TXRF instrument status and Figures of Merit (FOM) of analysis



- Spectrometer (amplifier) gain fixed at the start of every run through As K_{α} line gain correction

Calibration eqn:

$$E(\text{keV}) = 0.005004(\text{keV}/\text{ch}) - 0.4883 \text{ keV}$$

- Mn K_{α} 5.9 keV line FWHM throughout varied little: $\sim 140 \text{ eV}$ (30 mm² SDD)
- Sensitivity measured at Ni K_{α} ~ 46 counts/(ng.mA.s)

Figures of merit		
Precision	$P [\%] = 100 \% - CV[\%]$	P: Precision
Coefficient of Variation	$CV [\%] = \frac{\sigma_i}{\bar{x}_i}$	CV: Coefficient of Variation. σ_i : Standard deviation of the concentration of the i^{th} element. \bar{x}_i : Average value of the concentration of the i^{th} element.
Trueness	$T [\%] = \frac{\bar{a}^i}{a_{ref}^i} 100$	\bar{a}^i : average concentration of the i^{th} element calculated for all measurement series. a_{ref}^i : reference value of the concentration of the element in the SRM.
Limit of Detection	$LOD = \frac{3C_i\sqrt{N_{Bg}}}{N_i} \sigma_b$	C_i : Concentration of the i^{th} element in the sample. N_{Bg} : area of the background under K_{α} line for the analyte element. N_i : net area of the peak for K_{α} line of the i^{th} element. σ_b is the standard deviation of the background area
Recovery	$R [\%] = \frac{\bar{x}_{sm}}{x_s}$	\bar{x}_{sm} : Average value of the measured concentration of the standard element. x_s : Concentration of the element as prepared in the standard.

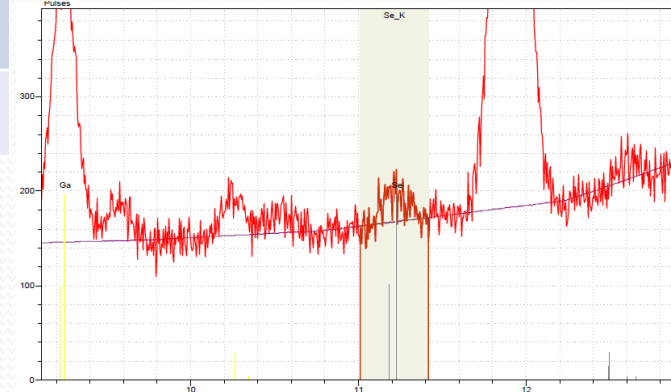
Sample FOMs and factors that affect the FOMs

Standard Conc. (mg/l)	Selenate in tri-distilled water				Selenate in AHU			
	Exptl. Value (mg/l)	% Recovery	% Precision	LLD (mg/l)	Exptl. Value (mg/l)	% Recovery	% Precision	LLD (mg/l)
0.01	0.039 ± 0.001	390 ± 10	98.50	0.001	0.007 ± 0.006	70 ± 0.6	98.30	0.001
0.1	0.063 ± 0.001	63 ± 1	99.00	0.001	0.117 ± 0.011	117 ± 11	97.10	0.001
1.0	0.881 ± 0.004	88.1 ± 0.4	99.60	0.02	1.570 ± 0.027	157 ± 2.7	98.70	0.02
10.0	8.960 ± 0.013	89.6 ± 0.13	99.90	0.02	10.490 ± 0.072	104.90 ± 0.72	99.60	0.02
100.0	96.876 ± 0.144	96.876 ± 0.144	99.99	0.012	-	-	-	-

Standard Conc. (mg/l)	Selenomethionine in tri-distilled water				Selenomethionine in AHU			
	Exptl. Value (mg/l)	% Recovery	% Precision	LLD (mg/l)	Exptl. Value (mg/l)	% Recovery	% Precision	LLD (mg/l)
0.01	0.007 ± 0.001	70	83	0.002	0.129	1290	98.2	0.001
0.1	0.102 ± 0.001	102	99.3	0.001	0.206	206	98.9	0.003
1.0	0.977 ± 0.004	97.7	99.6	0.001	0.982	98.2	99.1	0.006
10.0	10.231 ± 0.013	102.31	99.9	0.003	14.308	143.1	99.6	0.022

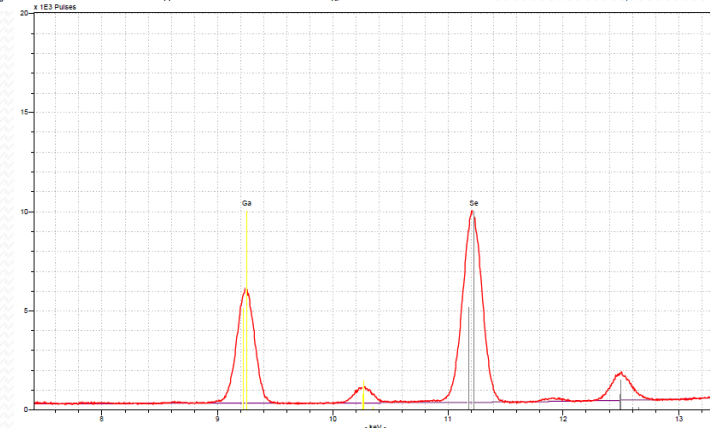
Sample stability over 6 months' storage @ 20 °C, mean RH ~ 30%

Standard conc. (mg/l)	Matrix	Analyte molecule	Exptl. Conc. (mg/l)	% Recovery	% Precision
10	Water	SeT	9.145 ± 0.016	91.45	99.8
		SeMet	10.116 ± 0.014	101.16	99.7
	AHU	SeT	5.711 ± 0.018	57.11	99.7
		SeMet	2.193 ± 0.010	21.93	99.5



0.01 mg/l SeM in AHU

10mg/l SeM in AHU



At standard concs. ≥ 0.1 mg/l the % recoveries are good but at < 0.1 mg/l, deviate substantially from 100%

- Poor S/N, over/under compensation of background of weak peaks by the global background fit of SPECTRA7 quantitative anal. software.
- Global background fit works well for strong peaks

Sample FOMs and Factors that affect the FOM

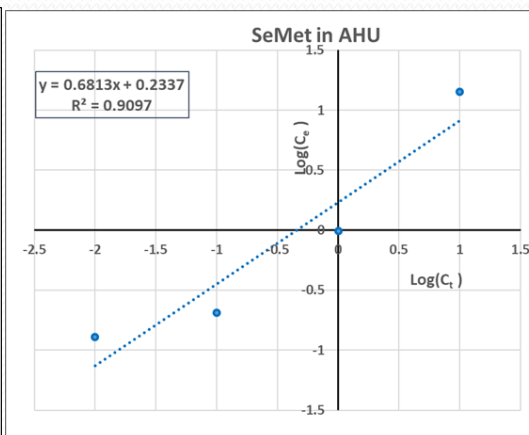
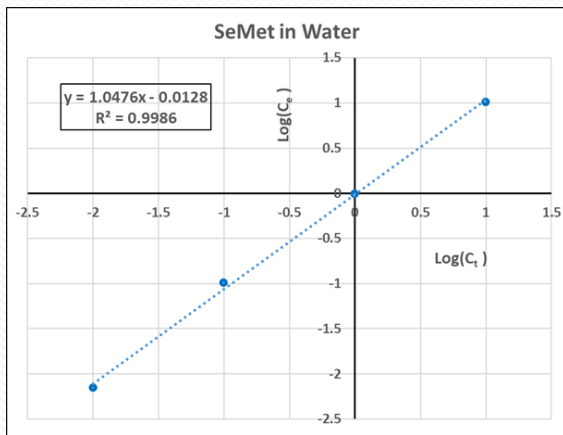
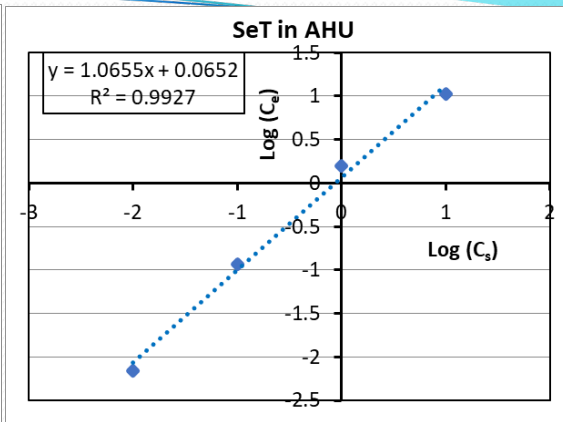
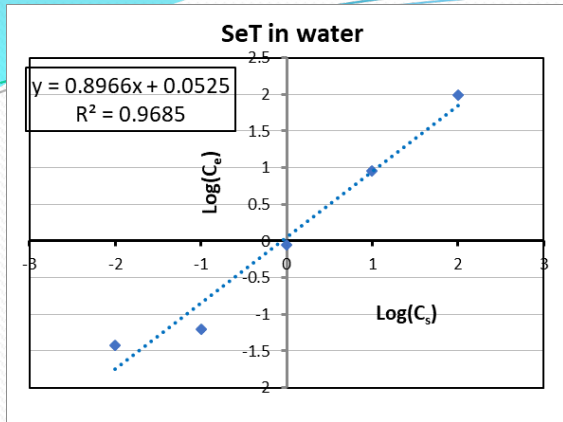
Three options to improve the % Recovery:

- Longer counting times to increase peak counts. Disadvantage: also increases the Bg counts
- Improved peak analysis software esp. background fits with AI to locate weak peaks that require customization of the global fit
- Sample prep technique that can enhance S/N; typical procedures such as preconcentration through heating a challenge and dubious for volatile elements/compounds or time-sensitive volatile compounds. Innovative ideas needed!

Sample stability over 11 months' storage @ 20 °C, mean RH ~ 30%					
Standard conc. (mg/l)	Matrix	Analyte molecule	Exptl. Conc. (mg/l)	% Recovery	% Precision
10	Water	SeT	9.145 ± 0.016	91.45	99.8
		SeMet	10.116 ± 0.014	101.16	99.7
	AHU	SeT	5.711 ± 0.018	57.11	99.7
		SeMet	2.193 ± 0.010	21.93	99.5

- To test sample temporal stability the 10 mg/l sample (good S/N) disc was re-run after 6 months. SeT and SEMet in water suffered little loss of recovery but the AHU based samples, esp. SeMet in AHU suffered ~ 80% loss. Possibly slow degradation of samples leading to Se volatilization in AHU matrix ~~aided by bacterial/fungal action.~~
- TXRF is a non-consumptive technique but the sample itself may be self-consumptive!
- Sample age and storage condition might be important for certain provenances e.g. forensic, geological, radioactive

Linear Dynamic Range (LDR)



- Linear range or linear dynamic range – The range of concentrations where the signals are directly proportional to the concentration of the analyte in the sample.

- The graphs and the calculations show that over 5 orders of magnitude of concentration the linearity between the experimental concentration C_e and standard concentration C_s is maintained.
 - Except for SeMet in AHU
 - Stronger matrix effects weaken the linear relationship.

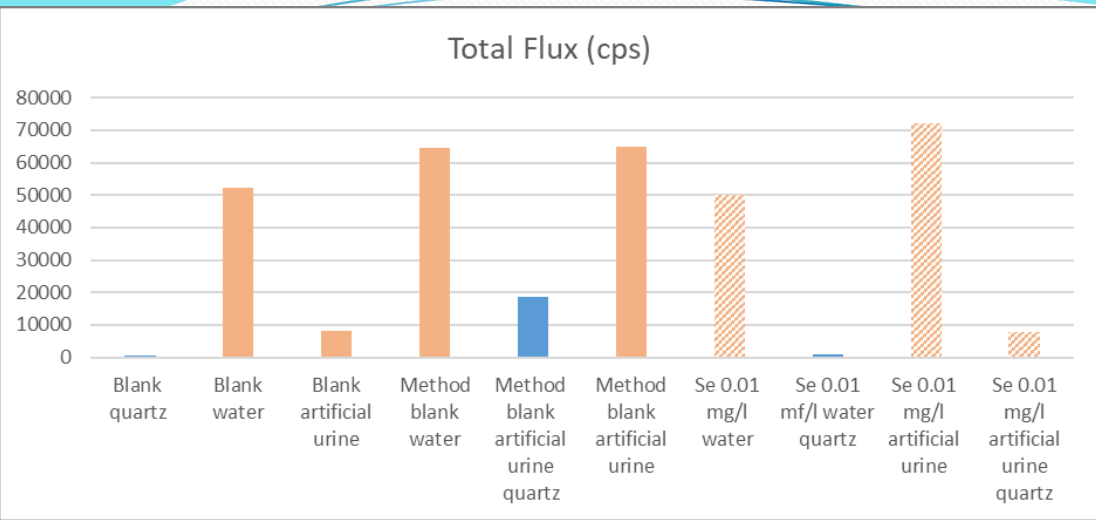
$$\log(C_e) = m \cdot \log(C_s) + c = m \cdot \log(C_s) + \log(C')$$

$$C_e / (C_s)^m = C' \Rightarrow (C_e / C_s) \approx C' \text{ since } m \approx 1 ;$$

$$C' \rightarrow 1 \text{ since } c \rightarrow 0$$

In a simple matrix TXRF shows an LDR of 5 orders of magnitude

Matrix Effects – Contributions of the Sample Carrier

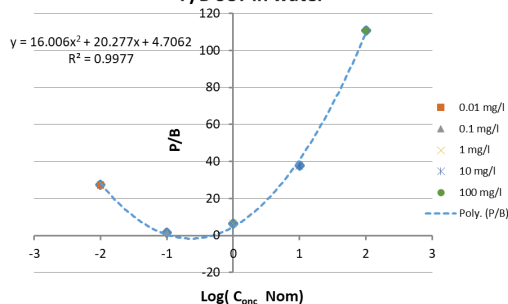


- The evanescent wave penetrates a few nm into the substrate/sample carrier: it contributes to the background (Bg)
- Bg contributions tested by discs +/- siliconization ('Blank'), --/+ solvent matrix (Water or AHU). -/+ the Ga IS ('Method Blank').
- Bg metric was the Total Photon Count (TPC) registered by the detector. In the ideal sample carrier Bg, TPC should be a minimum

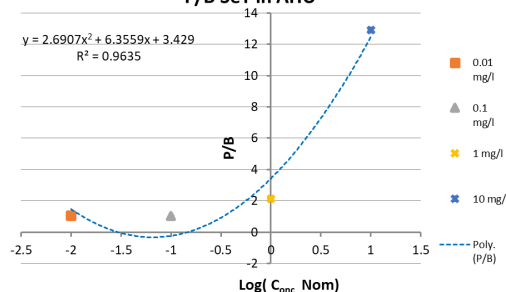
- Acrylic produces more TPC than quartz because of predominantly light element (C, H, O) composition -> **high Compton scattering of primary x-ray beam.**
- Introducing AHU reduces Compton flux by **matrix absorption** by the AHU's elements.
- Introducing Ga in water/AHU increases TPC by the large flux of fluoresced x-rays of Ga; less if quartz substrate used.
- This work used acrylic carriers - high cost of quartz carriers (in Mexico)

Matrix Effects: Contributions of the Analyte Matrix

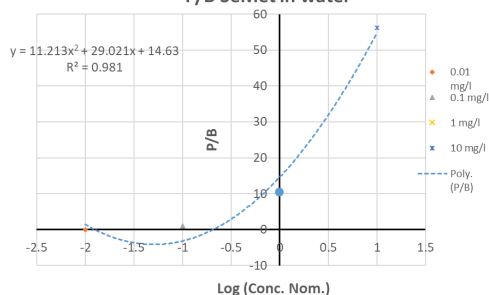
P/B SeT in water



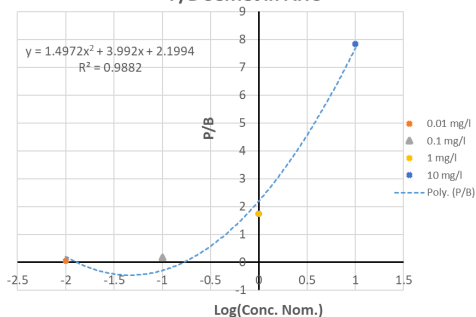
P/B SeT in AHU



P/B SeMet in water



P/B SeMet in AHU



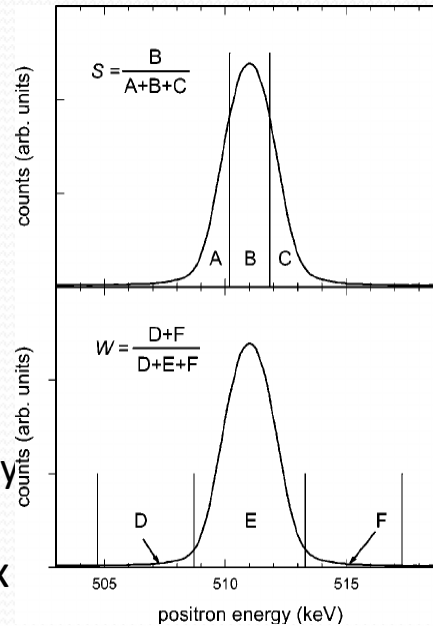
- Metric is the Peak to Background (P/B) ratio => signal “sensitivity”
- For a given matrix (solvent), the Bg would be a constant
- As the analyte concentration reduces, the Se XRF photon counts would decrease.
- The P/B should therefore monotonically decrease
- In figs 10.1 – 10.4 instead of continual decrease we have a parabolic response! At the lowest concentrations, ≤ 0.1 mg/l the P/B increases.
- In the Se analytes the self-absorption by Se would be the highest since it is the highest Z element there. At very low concentrations the substantial decrease of the self-absorption factor leads to the increase of P/B
- Could this phenomenon be leveraged to increase the sensitivity of Se at low (ppb) concentrations?

Matrix Effects: S, W and S/W Parameters

- Inspired by Doppler broadening Positron Annihilation Gamma Spectrometry (PAS)

Annihilation Gamma Spectrometry (PAS)

- S, W parameters of the 511 keV gamma peak used to ascertain open volume defects and the influence of the chemical environment, respectively



- To quantify the matrix effects we evaluated the S and W parameter for the K α Se line.
- S/W ratio combines the effects of S and W separately.
- A relatively high difference in S/W values occurs when the chemical matrix is changed (water vs AHU) but very little when the Se oxidation state and ligands in the Se molecule are changed (SeT_water, SeMet_water). Tallies with the Chem. Shift results.

Se @ 10 mg/l	S and W Parameters		S/W ratio
	ORIGIN9.1		ORIGIN9.1
	S	W	S/W
SeT_water	0.758	0.032	23.669
SeT_AHU	0.763	0.030	25.069
SeMet_water	0.757	0.033	23.015
SeMet_AHU	0.769	0.024	32.269

- This is a preliminary attempt to quantify matrix effects following the ansatz of PAS. More needs to be done to establish the ground.
- Both the Chem. Shift and S/W parameter give an insight into how the matrix interacts with the fluorescent emissions of the analyte atom.

Line-shape parameters of the Se K_{β} line

- Nearly the same effects are seen: the differences are more obvious for the analyte atom when encased in a different molecular structures and a different matrix.

Analyte	Medium	Concentration [mg/l]	Peak Energy [keV]	Se $K_{\beta 1}$ line* [keV]	$[\Delta E/E]10^{-4}$	FWHMS [keV]	W parameter	W parameter
SeT	Tri-distilled water	10	12.497	12.495	1.60	0.192	0.777	0.035
	Artificial Human Urine		12.500		4.00	0.197	0.764	0.031
Tri-distilled water	12.500		4.00		0.204	0.764	0.031	
Artificial Human Urine	12.505		8.00		0.257	0.781	0.005	

Conclusion

- TXRFS can be effectively used to analyze Se metabolites in simple (water) or complex (AHU) matrices with good FOMs over a large linear dynamic range. However, Se volatility in AHU matrix affects long-term sample integrity.
 - Chemical behaviour of the analyte atom needs to be taken into account for high precision x/gamma ray spectrometry
- Matrix effects limit the FOMs in the ultra-trace region
- Matrix and analyte atom bonding environments may perhaps be quantifiable in TXRF through probes such as Chemical Shift and the PAS inspired S/W parameter analysis. This work is exploratory but opens the door for more incisive investigation.



UNIVERSIDAD MICHOCANA
DE SAN NICOLÁS DE HIDALGO

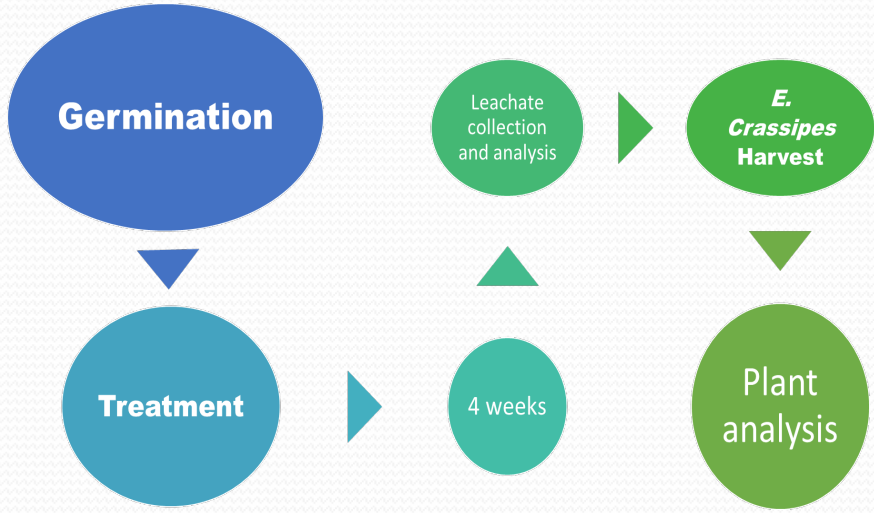
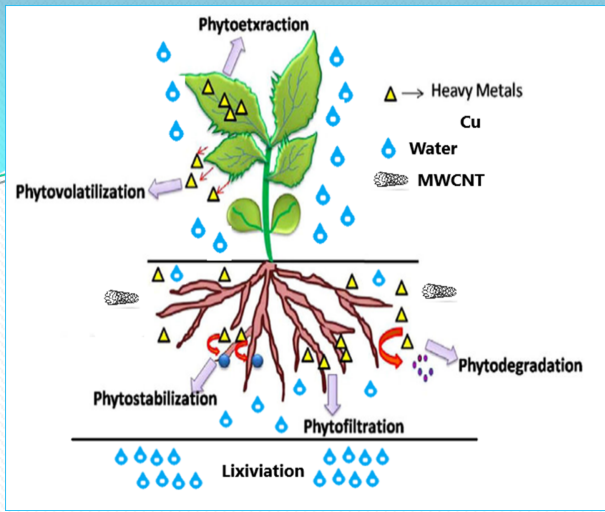
Plant tissue and soil leachate Cu(II) concentrations for copper contaminated soil amended by Carbon Nanotubes and Activated Carbon

Nabanita Dasgupta-Schubert

Department of Physics and Mathematics
University of Michoacan, Morelia, Mexico



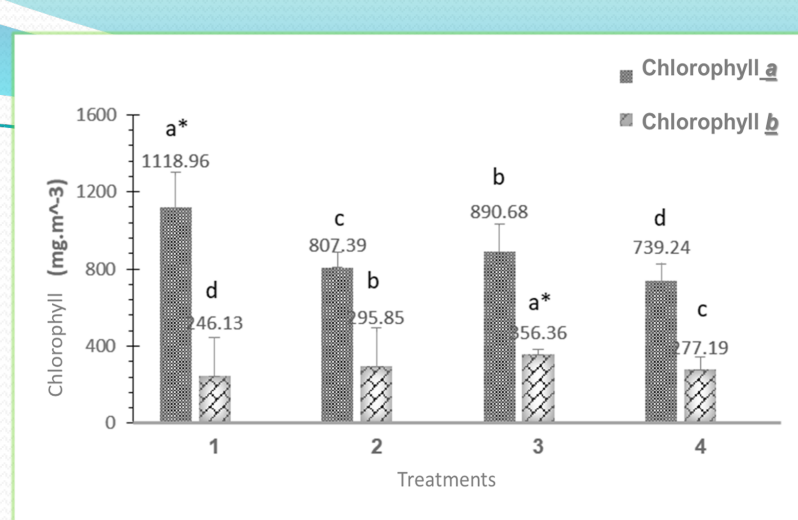
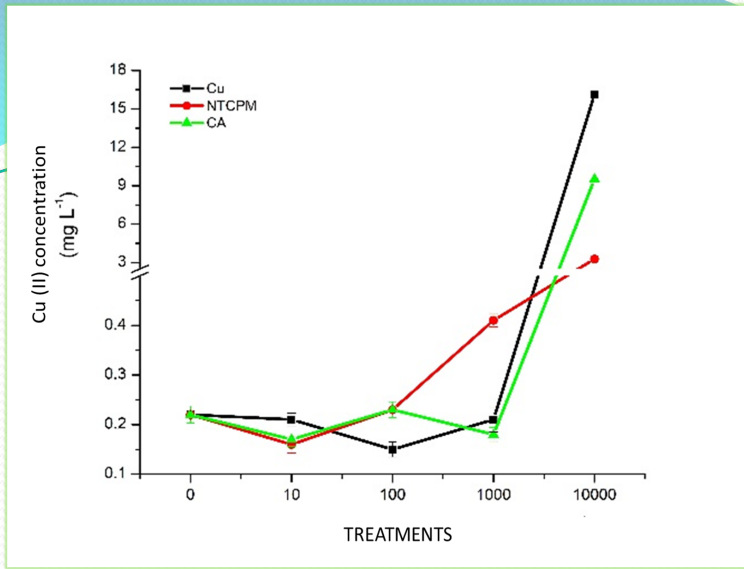
- Phytoremediation is a sustainable environmental biotechnology that remediates soil impacted by moderately high concentrations of organic and inorganic (chiefly heavy metal (HM)), pollutants using contaminant-accumulating plants.
- *Brassica juncea* (Indian mustard) is a copper hyperaccumulator (HA).
- A set of laboratory experiments under controlled conditions of temperature, relative humidity and photoperiod was carried out for the remediation of loamy soil contaminated by 10, 100, 1000 and 10,000 (mg/kg dry soil) of Cu(II) as Copper Oxochloride (Cupravit®) using *B. juncea* as phytoremediant.
- The soils had previously been amended separately by multiwalled carbon nanotubes (MWCNT) and by activated carbon (AC) both of > 95% purity and at 20mg/kg.
- Plant metal concentrations were analysed by TXRF spectrometry with the sample deposited as nearly a monolayer of ground plant dry matter, of particle size $\leq 88\mu\text{m}$.
- Plant leachates were analysed by FAAS
- The results will be analysed in terms of the mathematical r-K model developed by us.



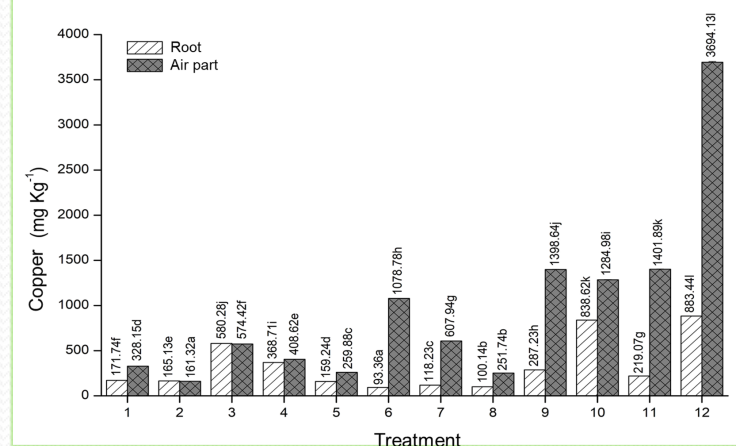
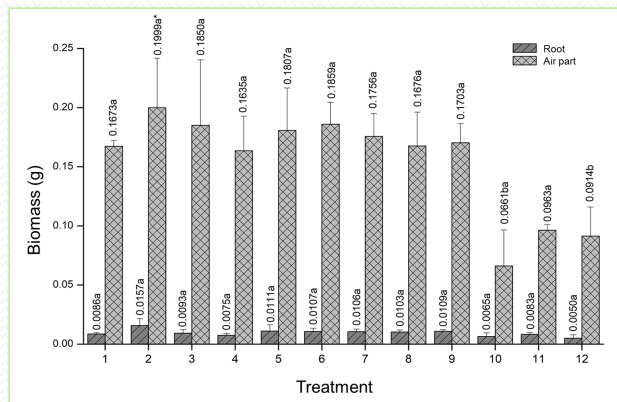
Experimental design of phytoremediation of a Cu (II) contaminated soil by *Brassica juncea* enhanced with MWCNT and AC.

Copper (II) concentration (mg/kg)	0	10	100	1000	10000
Control/Cupravit	NA	NA	NA	NA	NA
NTCPM (mg/kg)	20	20	20	20	20
Carbón activado (mg/kg)	20	20	20	20	20





• Figure 2. 1) Control. 2) In soil with 95% pure Multi-walled Carbon Nanotubes plus Copper 1000mg/Kg. 3) In soil with Activated Carbon plus Copper 1000 mg/Kg. 4) In soil with Copper 1000 mg/Kg. Tukey test (0.05)*. Equal letters show no significant difference.



• Figure 3. Dry weight of aerial part and root of Brassica juncea enhanced with MWCNT and AC in the phytoremediation of Cu (II) contaminated soil

• Figure 4. Cu (II) concentration in aerial and root part of Brassica juncea enhanced with MWCNT and AC in phytoremediation of Cu impacted soil.

Conclusion

- Overall, this work indicates that amending soils by low concentrations of MWCNT and AC could aid the phytoremediation of Cu.
- At high concentrations of Cu, the MWCNT treated soil aided plant growth and diminished dissolved Cu in soil run-offs (leachates) while the highest plant concentrations of Cu were obtained for the AC treated soils.
- Substantially higher Cu concentrations were found in the roots than in the aerial parts for all sets, but this was particularly marked for the soils amended by AC.
- Cu diminished both chlorophyll a and b but the application of MWCNT and AC slowed this diminution signifying an increased plant resilience to Cu toxicity.
- The powdered plant tissue samples tended to form islands (upon microscopic examination) on the TXRF sample substrates causing a relatively large standard deviation due to sample particle size and the resulting inhomogeneity effect.
- Nonetheless the average concentrations in the plant tissue for all sets seem to follow the r-K model of metal accumulation Cu polluted soils.

Acknowledgements

My doctoral students,

Waleed Amin Abuhani, Jorge Luis Rodríguez Alejandro and Iris Eunice Serrato Mireles of the Department of Physics and Mathematics of the University of Michoacan, Mexico,

And my collaborators,

Prof. Vivechana Agarwal of the Autonomous University of the State of Morelos (UAEM), Mexico, **Dr. Vijay Raj Sharma** of the INFN-LNS Catania, Italy, **Prof. Juergen Mattusch** of the Umweltforschung Zentrum, Leipzig, Germany, **Prof. Steve Alexander** of Southwestern University, Georgetown, TX, USA.

Funding for this work was provided by CONAHCyT of Mexico